



# mP-Gait: Fine-grained Parkinson's Disease Gait Impairment Assessment with Robust Feature Analysis

WENHAO ZHANG, Nanjing University, China

HAIPENG DAI\*, Nanjing University, China

DONGYU XIA, Nanjing University, China

YANG PAN, The affiliated Brain Hospital of Nanjing Medical University, China

ZESHUI LI, Nanjing University, China

WEI WANG, Nanjing University, China

ZHEN LI, The First Affiliated Hospital of Soochow University, China

LEI WANG, Soochow University, China

GUIHAI CHEN\*, Nanjing University, China

Patients with Parkinson's disease (PD) often show gait impairments including shuffling gait, festination, and lack of arm and leg coordination. Quantitative gait analysis can provide valuable insights for PD diagnosis and monitoring. Prior work has utilized 3D motion capture, foot pressure sensors, IMUs, etc. to assess the severity of gait impairment in PD patients. These sensors, despite their high precision, are often expensive and cumbersome to wear which makes them not the best option for long-term monitoring and naturalistic deployment settings. In this paper, we introduce mP-Gait, a millimeter-wave (mmWave) radar-based system designed to detect the gait features in PD patients and predict the severity of their gait impairment. Leveraging the high frequency and wide bandwidth of mmWave radar signals, mP-Gait is able to capture high-resolution reflected signals from different body parts during walking. We develop a pipeline to detect walking, extract gait features using signal analysis methods, and predict patients' UPDRS-III gait scores with a machine learning model. As gait features from PD patients with gait impairment are correctly and robustly extracted, mP-Gait is able to observe the fine-grained gait impairment severity fluctuation caused by medication response. To evaluate mP-Gait, we collected gait features from 144 participants (with UPDRS-III gait scores between 0 and 2) containing over 4000 gait cycles. Our results show that mP-Gait can achieve a mean absolute error of 0.379 points in predicting UPDRS-III gait scores.

CCS Concepts: • Human-centered computing → Ubiquitous and mobile computing systems and tools.

Additional Key Words and Phrases: Parkinson's Disease, mmWave radar, gait analysis, fine-grained assessment

---

\*Corresponding authors are Haipeng Dai and Guihai Chen

---

Authors' addresses: [Wenhao Zhang](#), Nanjing University, No.163 Xianlin Avenue, Qixia District, Nanjing, China, DZ20330040@mail.nju.edu.cn; [Haipeng Dai](#), Nanjing University, No.163 Xianlin Avenue, Qixia District, Nanjing, China, haipengdai@mail.nju.edu.cn; [Dongyu Xia](#), Nanjing University, No.163 Xianlin Avenue, Qixia District, Nanjing, China, qfwfq42@mail.nju.edu.cn; [Yang pan](#), The affiliated Brain Hospital of Nanjing Medical University, No.264 Guangzhou Road, Gulou District, Nanjing, China, panyangubicomp@163.com; [Zeshui Li](#), Nanjing University, No.163 Xianlin Avenue, Qixia District, Nanjing, China, dg1633010@mail.nju.edu.cn; [Wei Wang](#), Nanjing University, No.163 Xianlin Avenue, Qixia District, Nanjing, China, ww@mail.nju.edu.cn; [Zhen Li](#), The First Affiliated Hospital of Soochow University, No.188 Shizi Street, Suzhou, China, drlizhen2021@163.com; [Lei Wang](#), Soochow University, Suzhou, China, wang\_l@pku.edu.cn; [Guanghai Chen](#), Nanjing University, No.163 Xianlin Avenue, Qixia District, Nanjing, China, gchen@mail.nju.edu.cn.

---

Permission to make digital or hard copies of all or part of this work for personal or classroom use is granted without fee provided that copies are not made or distributed for profit or commercial advantage and that copies bear this notice and the full citation on the first page. Copyrights for components of this work owned by others than the author(s) must be honored. Abstracting with credit is permitted. To copy otherwise, or republish, to post on servers or to redistribute to lists, requires prior specific permission and/or a fee. Request permissions from [permissions@acm.org](mailto:permissions@acm.org).

© 2024 Copyright held by the owner/author(s). Publication rights licensed to ACM.

2474-9567/2024/9-ART142

<https://doi.org/10.1145/3678577>

**ACM Reference Format:**

Wenhai Zhang, Haipeng Dai, Dongyu Xia, Yang pan, Zeshui Li, Wei Wang, Zhen Li, Lei Wang, and Guihai Chen. 2024. mP-Gait: Fine-grained Parkinson's Disease Gait Impairment Assessment with Robust Feature Analysis. *Proc. ACM Interact. Mob. Wearable Ubiquitous Technol.* 8, 3, Article 142 (September 2024), 31 pages. <https://doi.org/10.1145/3678577>

## 1 INTRODUCTION

Parkinson's disease (PD) is the second most prevalent neurodegenerative disorder in the world [19]. It causes the demise of dopamine-producing neurons in the substantia nigra. Consequently, with the reduction of dopamine, the signals responsible for movement control cannot be entirely relayed to other brain regions. This results in the four primary symptoms of PD: resting tremor, rigidity, bradykinesia, and postural instability [31]. Among these symptoms, gait impairment caused by bradykinesia and postural instability is the most common. In clinical diagnosis, gait impairments are typically observed and quantified using phenotypic tests [22]. For example, the Hoehn-Yahr scale and UPDRS score are used to measure the development of PD [20, 45]. However, these evaluation methods are inherently subjective and different doctors may give inconsistent scores. Therefore, there have been many efforts to use various kinds of sensors to measure patients' gait features and assess their gait impairment severity.

Existing work assesses patients' gait impairment severity through gait features collected by 3D motion capture systems [2, 3, 27, 55], foot pressure sensors [49, 56], IMUs [5, 17, 37, 66], etc. These devices require the patients to wear additional devices or even tight-fitting suits with markers during measurements. While these sensors are highly accurate in obtaining patients' gait features and assessing the gait impairment severity, they are primarily suited for one-time assessment in the controlled environment, such as a hospital's examination room, rather than for monitoring gait changes over time in daily life.

Monitoring temporal changes in patients' gait can provide meaningful insights for doctors to assess disease progression and medication effects because gait patterns can be changed by medication [6]. Medications are used to mitigate the effects of PD on patients' daily lives and decelerate symptom exacerbation [43]. PD patients commonly take medications like levodopa to alleviate symptoms [40]. These medications enhance dopamine levels in the brain, thus diminishing PD symptoms during their effective phases. However, the additional dopamine intake can lead to pronounced fluctuations in dopamine levels among patients. This is possible to cause dopamine peaks or even levodopa-induced dyskinesia which can exacerbate gait impairment and reduce patients' quality of life [34]. Optimizing medication dosage and intervals can reduce dopamine peaks. However, different patients' sensitivity varies for different medications, so determining suitable medication types, dosages, and timings remains important [24].

Currently, doctors rely on patients' self-reported medication responses to adjust the dosages and medication types, which are subjective. Quantitative gait features over time can reflect changes in patients' gait patterns after medication and the effective durations of such medication. This information is crucial for doctors to comprehend the medication's impact on patients. What's more, for patients whose gait impairment severity changes slightly before and after medication, the changes in their gait features are correspondingly subtle. Therefore, fine-grained assessment of gait impairment severity is equally important for assisting doctors in evaluating medication effects. However, while doctors can assess the severity of PD patients' gait impairment using the UPDRS-III gait score scale (shown as Table 1), quantifying those patients with gait scores of 1 and 0.9 is still challenging due to the coarse granularity of the scale.

Since gait features over time are the data we require, the data collection method should be convenient and simple. Non-contact sensors provide a potential solution. Prior works using non-contact sensors like cameras [13, 35, 38] or Kinect [54] are susceptible to lighting conditions, have limited coverage range, and infringe on patients' privacy. Although acoustic or RF signals [21, 30, 57, 62, 65] have proven to be able to analyze gait patterns, previous work mainly focused on healthy people's gait in laboratory settings or PD patients' primary

Table 1. UPDRS-III Gait Score Scale

UPDRS-III Gait Score	Corresponding Gait Features
0-Normal	Normal.
1-Slight	Walks slowly, may shuffle with short steps, but no festination (hastening steps) or propulsion.
2-Mild	Walks with difficulty, but requires little or no assistance; may have some festination, short steps, or propulsion.
3-Moderate	Severe disturbance of gait, requiring assistance.
4-Severe	Cannot walk at all, even with assistance.

gait features like stride length and gait velocity. More features are required for fine-grained gait impairment severity assessment.

We envision a novel system that can conveniently collect patients' gait features with high accuracy and efficiency. It allows doctors to quickly understand patients' current gait status and assists doctors in evaluating gait impairment severity. Moreover, the convenient data collection and the fine-grained gait impairment severity assessment ability mean that doctors can obtain large amounts of gait features varying over time, along with subtle changes in patients' gait patterns. In this way, the medication types, dosages and scheduling can be adjusted through the analysis of patients' gait changes over time. Specifically, we believe such a system should have the following characteristics:

- Convenient data collection: No extra devices are required for patients. They only need to walk as usual during data collection. Also, the process shouldn't be affected by environmental conditions like lighting and room layout which ensures flexible deployment in both hospital wards and patients' homes.
- High accuracy of collected data: The collected gait features should have high precision, allowing doctors to observe subtle changes.
- Robust to gait impairment: PD patients often have shuffling gait, festination, and lack of arm and leg coordination. The system should extract correct gait features without being affected by these conditions.
- Sensitive to changes in gait pattern: For PD patients with small changes in gait features before and after medication, the severity changes of their gait impairment should also be assessed correctly.

We introduce and implement mP-Gait for the acquisition of gait features in PD patients and the subsequent prediction of their gait impairment severity. For data collection convenience, we only consider non-contact sensors. Among them, although acoustic signal offers superior range resolution due to the slower propagation speed, its coverage range is shorter compared with RF signals, resulting in restricting its ability to detect walking patients except at relatively close distances. For RF signals, mmWave radar is selected for its high frequency and wide bandwidth, enabling highly accurate distance and velocity resolution. Meanwhile, mmWave radar can cover a range of approximately 12 meters [4], which is sufficient for common medical gait testing methods such as TUG (Timed Up and Go Test) [51] and 10MWT (10 Meter Walk Test) [29].

We collect the reflected mmWave radar signals from walking patients, and use signal processing methods to calculate the signal variations caused by human body. From the received signals, we extract primary gait features like stride length, gait velocity, step duration, etc. These quantitative gait features can help doctors understand patients' current gait status objectively through data rather than subjective judgments. Moreover, we extract periodic patterns from the processed signals as extended gait features, which can reflect gait status as well. Combining all these features, we input them into a regression model to predict patients' UPDRS-III gait scores and assist doctors in assessing fine-grained gait impairment severity.

To obtain real-world PD gait features, we collaborated with medical experts to collect data in clinic rooms, wards, conference rooms, etc. Participants were asked one by one to walk a 5m distance individually back and forth twice in front of the deployed radar. In this way, we were able to collect gait data and doctors' given scores from 144 participants (65 patients with UPDRS-III gait score=0, 51 patients with UPDRS-III gait score=1, and 28 patients with UPDRS-III gait score=2) with more than 4000 gait cycles. We only chose patients with UPDRS-III gait scores from 0 to 2 as our participants, because based on the scale outlined in Table 1: For patients with UPDRS-III gait score=4, they cannot walk at all, even with assistance. So it is not possible to collect their gait data. And for patients with UPDRS-III gait score=3, they require assistance to walk. However, whether the patients are under the support of caregivers, or using tools like walkers, the "assistance" that the patients receive cannot be quantified. Moreover, patients with UPDRS-III gait score=3 have a high risk of falling when walking. Thus, we did not collect data for patients with UPDRS-III gait scores greater than 2 in our dataset.

Results show that mP-Gait can achieve a mean absolute error of 7.63 cm in stride length calculation and 0.096 s in step duration calculation. Furthermore, it attains a mean absolute error of 0.379 points in predicting UPDRS-III gait scores in comparison with the assessments provided by doctors. While the precision of gait scoring predictions may not reach the levels of 3D motion capture systems, mP-Gait effectively detects subtle changes in PD patients' gait patterns. Our system is able to track the changes in gait scores, particularly detecting improvements in gait impairment severity after medication, followed by a gradual decline in effectiveness as the medication loses its efficacy.

We conclude our contributions as follows:

- To the best of our knowledge, we are the first to use COTS mmWave radar for PD gait analysis and extract quantitative gait features, enabling convenient data collection without affecting patients or infringing on privacy. Doctors can observe subtle gait pattern changes before and after medication through frequent data collection.
- We design a gait segmentation algorithm to extract gait features from PD patients, robust to gait impairment like shuffling gait, festination, and lack of arm and leg coordination, etc.
- In addition to primary gait features like stride length and step duration, we extract extended gait features through time-frequency analysis. Based on all gait features, we train a regression model to predict fine-grained UPDRS-III gait scores.
- We collect gait data from participants with different gait impairment severity (UPDRS-III scores ranging from 0 to 2) and healthy controls in real hospital settings to evaluate mP-Gait's performance on real-world mmWave radar data.

## 2 RELATED WORKS

In this section, we briefly review existing solutions for PD gait impairment diagnosis using wearable or non-contact devices and gait analysis methods with the potential.

### 2.1 PD Gait Diagnosis with Wearable Devices

Gait diagnosis systems use wearable devices, such as tight-fitting suits with markers in 3D motion capture, foot pressure insoles, or IMUs attached to legs, to capture gait signals.

Although a 3D motion capture system (such as Vicon) requires the attachment of markers to the patient's body to monitor spatial position changes, it has the best accuracy with the high-precision sensors used. Wahid et al. [55] gathered stride length, cadence, stance time, and double support time from Vicon and force-plate. Employing a Random Forest algorithm, they got a PD classification accuracy of 92.6%. Kwon et al. [27] used 3D motion capture data and trained an attention-based adaptive graphical convolutional network to predict the FOG score and MDS-UPDRS total score. They achieved 97.6% accuracy in predicting the FOG score and an error of less than 2.7 points in the MDS-UPDRS score.

The method based on ground reaction force requires the patients to walk on a pre-arranged pressure plate or wear specialized foot pressure insoles [68]. Because it is not easy for PD patients to put on and take off insoles, and customizing insoles for patients with different shoe sizes is costly, pressure plates are more widely used. Wang et al. [56] predicted the Hoehn and Yahr scale score for PD patients using vertical ground reaction force data collected from 8 sensors placed under each foot, achieving a prediction accuracy of 96.69%. Slijepcevic et al. [49], on the other hand, successfully classified different gait disorders with an accuracy above 80% by analyzing data from centrally embedded force plates.

IMUs are capable of obtaining precise acceleration and angular velocity of the patient's joints throughout the walking process. Han et al. [16] extracted twelve gait features from two shank-mounted IMUs to assess the MDS-UPDRS score and achieved 84.9% accuracy. Hasegawa et al. [17] attached the IMUs to patients' feet, shins, wrists, sternum, and lumbar region to collect data and successfully distinguish PD patients from healthy individuals with an accuracy of 82.4%.

With the ubiquity of smartphones, the integrated IMUs within these devices are also used to detect PD gait. Abou et al. [1] explored the use of smartphones' built-in IMUs for detecting gait dysfunctions and balance impairments, which are significant risk factors for falls and are associated with a diminished quality of life in individuals with PD. Capecci et al. [7] confirmed the reliability of leveraging smartphone-integrated IMUs for the detection of Freezing of Gait (FOG). Chomiak et al. [9] proposed a novel pattern recognition algorithm for the automated detection of gait-cycle breakdown and freezing episodes using Ambulosono smartphone-sensor technology.

PD gait diagnosis utilizing wearable devices have shown promising performance. However, these methods, relying on high-precision sensors, all have their own limitations: 3D motion capture systems and pressure plates are very expensive and virtually immobile once installed. IMUs and foot pressure insoles require patients to wear additional equipment which causes trouble to put on and affects their natural walking pattern to some degree.

## 2.2 PD Gait Diagnosis with Non-contact Devices

Diagnosing PD gait using cameras and Kinect is similar to using a 3D motion capture system, but does not require so many cameras to record or markers attached on patient's body. Through computer vision methods, the 3D human skeleton is reconstructed from video and depth sensor data, and the spatial position changes across various joints of the human body over time can be obtained. Endo et al. [13] employed VIBE (Video Inference for Body pose and shape Estimation) to extract 3D skeleton sequences from videos and proposed a deep learning method to predict UPDRS gait score, achieving an F1 score of 0.76. Krajushkina et al. [26] explored the use of Kinect for gait feature extraction to distinguish PD patients from health controls, reporting accuracy rates ranging from 0.71 to 0.85.

Computer vision-based methods face significant challenges as well: cameras are easily affected by light and have privacy infringements. Moreover, because reconstructing the human 3D skeleton from images already introduces errors, the body joints' motion data cannot achieve a promising accuracy either. Alternative computer vision-based methods that do not utilize cameras also have their drawbacks. The Kinect system, with its integrated depth sensor, offers a slight enhancement in accuracy, yet its tracking coverage is restricted to a range of 1.2-3.5m [58]. The infrared thermal imaging technique can identify gait patterns and has the potential for PD gait diagnosis, but it is not sensitive to participants wearing heavy coat [64].

## 2.3 Gait Analysis Methods

In addition to the aforementioned devices, wireless sensor-based methods are also taken into consideration for gait analysis, leveraging technologies such as Wi-Fi signals [57, 63], acoustic signals [28, 62], and mmWave radar signals [36, 65]. Devices which can send and receive Wi-Fi signals are the most widely deployed in daily life, but

Wi-Fi CSI based approach has its weaknesses: common COTS Wi-Fi devices' signal frequency and bandwidth is much lower than that of commercial mmWave radars, which leads to lower range and velocity resolution. Also, Wi-Fi CSI is sensitive to multi-path effects making it susceptible to the environmental changes. Acoustic-based methods are low-cost and highly available either, but the acoustic signal can only perceive the gait of the patient within a limited distance because it is propagated through vibrations. The mmWave radar which can provide high-resolution object motion information due to its high center frequency and large bandwidth, shows the best potential for PD gait diagnosis.

Seifert et al. [47, 48] explored how to distinguish limping gait from normal gait with Doppler radar. Through the implementation of the proposed cadence-velocity diagram, a qualitative assessment of the severity of patients' gait impairments can be conducted. Jiang et al. [25] proposed a human gait classification and recognition method based on a multi-channel three-dimensional convolution neural network with mmWave radar, achieving an accuracy exceeding 92.5% for distinguishing between common gait types such as jogging and normal walking. Zhao et al. [67] introduced a human tracking and identification system (mID) that employs a deep recurrent network to accurately identify individual users, demonstrating median positioning errors of 0.16m and correct identification rate of 89% for 12 people.

Current mmWave-based methods have succeeded in performing quantitative analysis on healthy people and qualitative analysis on simulated patients with gait disorders. However, conducting quantitative analysis on actual patients with gait impairments in real-world scenarios remains to be a challenge. In this paper, we introduce a novel approach for gait signal analysis to overcome the lack of robustness in conventional methods and demonstrates the potential of mmWave signals in predicting fine-grained UPDRS-III gait scores.

### 3 SYSTEM OVERVIEW

In this section, we present an overview of mP-Gait, including its application scenarios, the dataset we collected, and the system diagram (see Figure 1).

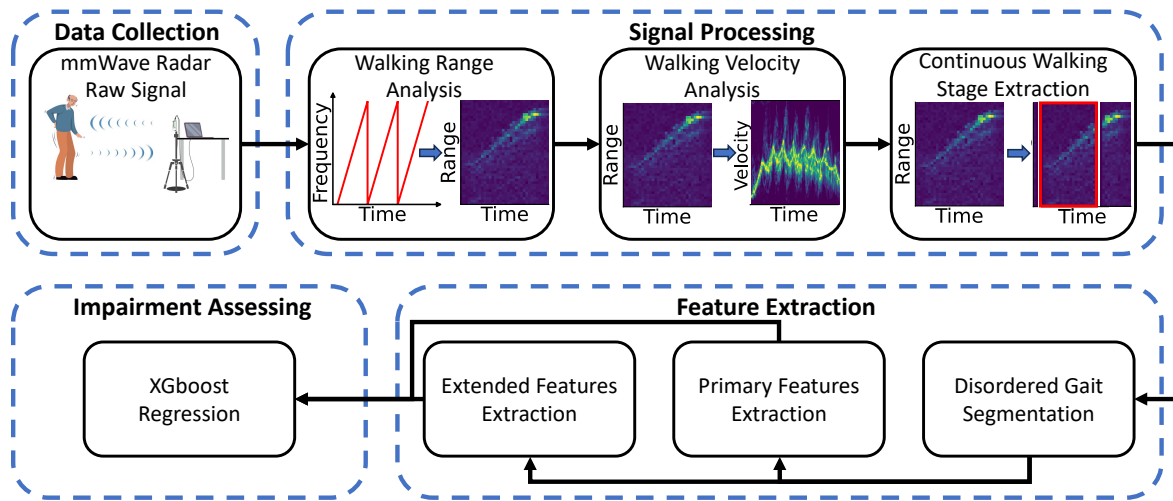


Fig. 1. The mP-Gait framework contains four modules: data collection, signal processing, feature extraction, and impairment assessment. The data collection module is accomplished by the radar end, which transmits and receives FMCW signals to record the whole walking pattern. The remaining modules are accomplished by the PC end, which processes the received signals, extracts gait features, and finally predicts the gait impairment severity using a machine learning model.

### 3.1 Motivation

The gait impairment is an important indicator for assessing the severity of PD. The walking pattern of PD patients is characterized by slow, short shuffling steps [52], freezing [15], lower limb muscle weakness [12] and reduced joint range of motion [11, 46] which cause the PD patients' gait features like stride length and gait velocity show a significant reduction and increased variation compared with health controls [18, 50].

Although medications appear to have limited efficacy in decelerating the progression of PD, they play an important role in mitigating the impact of gait impairment on patients' quality of life as a palliative management [43]. However, medications like levodopa are possible to cause dopamine peaks [34] which requires doctors to adjust medication dosage and frequency to avoid [24]. Doctors must monitor the changes in PD patients' gait before and after medication to assess its effects, but manual observation with high frequency is a huge burden for doctors and the result is easily influenced by their subjective judgment. Even though automated collection of gait features offers quantitative data, existing work using wearable devices requires specialized rooms and professional assistance to help patients put the devices on and collect data which is still inconvenient. As a result, doctors currently mainly rely on patients' subjective self-reports to evaluate medication effects.

### 3.2 Application Scenario

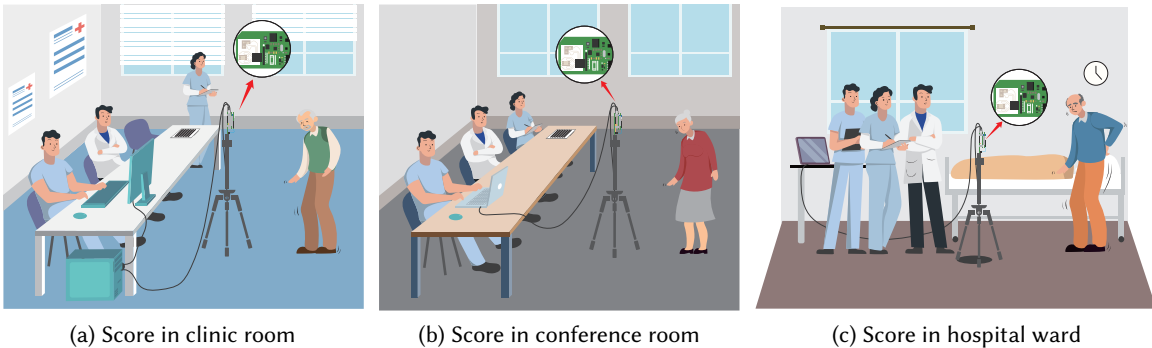


Fig. 2. The PD patients walking in front of the mmWave radar while the doctors considering the UPDRS-III gait score.

mP-Gait offers a user-friendly and easily deployable method for collecting gait features, benefiting both doctors and PD patients. It supports flexible deployment in various scenarios such as outpatient clinic rooms, conference rooms, or hospital wards, as shown in Figure 2. The patients are simply required to walk back and forth in front of the mmWave radar, with no difference from a normal walking process, for a duration of 1 to 2 minutes during which their gait signals are recorded. The collected signals will be analyzed by mP-Gait, so that doctors can obtain the patients' gait features and predicted UPDRS-III gait scores. Doctors can thus collect gait features before and after medication, assess feature changes, and select the best medication types, dosages, and dosing intervals to mitigate PD symptoms and decelerate patients' PD progression [43].

### 3.3 mP-Gait Overview

**Data collection:** We use a mmWave radar to transmit FMCW signals for detecting gait patterns. PD patients are instructed to walk back and forth in front of the mmWave radar, thus the raw RF signals containing the gait information of the PD patients are collected.

**Signal processing:** Leveraging the characteristics of the received raw RF signals, we use a method based on time-frequency analysis to obtain spectral information such as the range profile and the Doppler profile which can describe the changes in the walking process over time. Also, the data we collect includes a small period of standing time before the patient starts walking, turning time, and a small period of standing time after completing the walking process. We use the micro-Doppler profile to select the actual walking stages of the participants for further analysis.

**Feature extraction:** First, we design a robust algorithm to segment each step of the walking process to obtain the time and spectral feature changes for each step. Subsequently, these spectral changes are analyzed to calculate the primary gait features, including stride length, gait velocity, and step duration, etc. Finally, through detailed observation on spectra, we calculated extended gait features to better characterize gait patterns.

**Gait impairment assessment:** In order to assist doctors in evaluating the patient's gait impairment severity, we train a regression model to predict the UPDRS-III gait score using the extracted gait features. We also analyze the regression results and find that the max stride length in the second pass is the most indicative features for gait impairment assessment.

## 4 SYSTEM DESIGN

In this section, we describe the details of the mP-Gait system. We first introduce the mmWave radar signals used in the system and the signal processing methods designed for the received signals. Then, we propose a specially-designed feature extraction algorithm which is robust to PD gait disorder patients. Next, we extract gait information including stride length, gait velocity, step duration, etc. Finally, we introduce the training and optimization process of the regression model used by the system.

### 4.1 Signal Processing

**4.1.1 Transmitted and Received Signal.** Walking is a complex, coordinated activity engaging multiple body parts, including the torso, legs, feet, and arms. Throughout the walking process, different parts of the body move at different distances with their own speeds. Therefore, the signals we used are expected to be able to separate the targets with different speeds at different locations at the same time. mP-Gait uses FMCW signals, also known as chirp signals, to achieve this goal.

In our system, the radar is set to cyclically transmit the same chirp signal. The chirp is defined by a starting frequency  $f_c$ , duration  $T_c$ , and bandwidth  $B$ . Because the frequency of the chirp signal changes linearly, the slope representing the rate of change of the chirp frequency is  $S = B/T_c$ . Based on the above parameters, we can obtain the transmitted signal  $S^{tx}$  within  $T_c$ :

$$S^{tx}(t) = A^{tx} e^{j2\pi(f_c + \frac{B}{T_c}t)t}, 0 \leq t < T_c \quad (1)$$

where  $A^{tx}$  represents the amplitude of the transmitted signal. The receiving antenna captures the RF signal reflected by the object. Considering the time taken for RF signal propagation, the received signal can be treated as a delayed version of the transmitted signal. Meanwhile, the distances between radar and different objects vary from each other which causes the received signal to have different amplitudes and delays. With the received (RX) and transmitted (TX) signals, the mixer generates the intermediate frequency (IF) signal:

$$S^{IF}(t) = \sum_{i=1}^N A_i e^{j2\pi(f_c + \frac{B}{T_c}t)\tau_i}, t = 0, \frac{1}{N_r}T_c, \frac{2}{N_r}T_c, \dots, \frac{N_r - 1}{N_r}T_c \quad (2)$$

where  $A_i$  and  $\tau_i$  is the amplitude and delay of the signal reflected by  $i$ th object,  $N_r$  is the number of discrete points that the mmWave radar collect in  $T_c$  (decided by the sampling rate of the analog-to-digital converter data acquisition board). Since we know that the propagation speed of mmWave is  $c$  (speed of light), the distance between  $i$ th object and the mmWave radar can be obtained through  $\frac{\tau_i c}{2}$ .

**4.1.2 Walking Range Analysis.** As described in Section 4.1.1, we know that the distance between the  $i$ th object and the mmWave radar is determined by  $\frac{\tau_i c}{2}$ . However, for each received chirp, the reflection information of different objects cannot be separated. Although static objects' reflection information can be removed by eliminating the static component, the distances from different parts of the human body to the radar are also different. According to Equation (2), we can find that the delay of different objects  $\tau_i$  is related to the frequency of the IF signal. Therefore, we conduct the Fast Fourier Transform (FFT) on the IF signal to analyze its frequency. When a target appears in the radar's field of view, its large energy reflection accumulated over time will lead to a strong frequency response in the IF signal frequency spectrum, and the peak bins indicate the distances of the target's various parts. When performing FFT on  $N_s$  chirps, we can get a range profile  $RP(r, t)$  whose shape is  $N_r \times N_s$ . If the radar collects  $N_c$  chirps per second, with the known speed of mmWave  $c$ ,  $abs(RP(r_0, t_0))$  represents the reflected energy amplitude of the target at the range of  $\frac{r_0 c}{2B}$ , time of  $\frac{t_0}{N_c}$ .

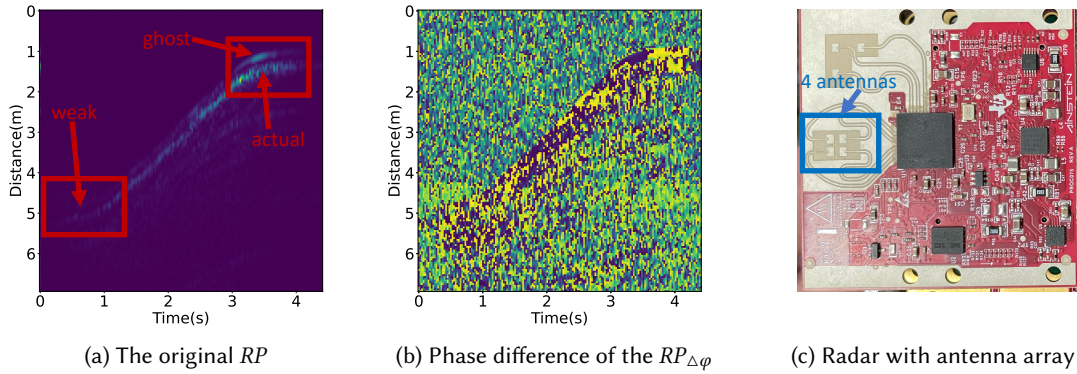


Fig. 3. Comparison between the  $RP$  and the  $RP_{\Delta\phi}$ .

Existing work typically identifies the bin with the maximum energy in the  $RP$  at each time to track the moving target [65]. However, as shown in Figure 3(a), when the walking patient is around 5 meters away from the mmWave radar, the weakening effect can be observed. This results from the reduced reflective surface area of the human body (compared with the reflective area of body when the patient is close to the radar), as well as the natural decay of radar reflection energy with increasing distance. When the weakening effect happens, because of the smaller reflection energy from the human body, the bin in  $RP$  with the maximum energy often corresponds not to the human body but to environment noise. What's more, when the walking patient is around 1 meter away from the mmWave radar, there occurs the ghosting effect due to the presence of both line-of-sight (LOS) signals and reflections via non-line-of-sight (NLOS) paths. In this way, the bin in  $RP$  with the maximum energy may be from either the LOS or NLOS path. Therefore, relying solely on the  $RP$  is insufficient for gait range analysis.

Generally speaking, mmWave radar has more than one receiving antenna (shown as Figure 3(c)). Thus, it is feasible to utilize the antenna array of the mmWave radar to supplement range information. Because of the spatial arrangement of the antenna array, the signals reflected from the same target arrive at different receiving antennas with different time delays. Considering the tiny distance difference between different receiving antennas to the target (less than 1/2 wavelength), the signals received by different antennas will have different phases in range profiles and range doppler profiles after signal processing.

If we consider that the signal comprises reflections from moving objects (dynamic component) and static objects (static component). For a static object  $OBJECT_0$  (e.g. table, chair, wall) at position  $r_0$  at time  $t_0$ . Although  $RP_{antenna1}(r_0, t_0)$  and  $RP_{antenna2}(r_0, t_0)$  are different, the distance changing of  $OBJECT_0$  relative to antenna1

and antenna2 is the same (no change). So by removing the static component, the dynamic component's phase difference between  $RP_{antenna1}^{dynamic}(r_0, t_0)$  and  $RP_{antenna2}^{dynamic}(r_0, t_0)$  is close to 0. However, for a moving object  $OBJECT_1$  (e.g. patient) at position  $r_1$  at time  $t_1$ , the distance changing of  $OBJECT_1$  relative to antenna1 and antenna2 is different. In this way, there will be a specific phase difference between  $RP_{antenna1}^{dynamic}(r_1, t_1)$  and  $RP_{antenna2}^{dynamic}(r_1, t_1)$  related to the moving direction of the object after removing the static component.

That is to say, static and moving objects have different phase differences in the  $RP$  received by different antennas, so we use the range phase difference profile  $RP_{\Delta\varphi}$  as supplementary information for gait range analysis, and its specific calculation is as follows:

$$RP_{\Delta\varphi}(r, t) = \text{phase}(RP_{antenna1}^{dynamic}(r, t)/RP_{antenna2}^{dynamic}(r, t)) \quad (3)$$

As shown in Figure 3(b), The range phase difference profile can provide corresponding range information no matter whether the participant is near or far from the radar. In Section 4.2.2, we will provide a detailed explanation of how to use  $RP$  and  $RP_{\Delta\varphi}$  to better locate the patient's position.

**4.1.3 Walking Velocity Analysis.** The range profile can identify targets at different ranges, but cannot distinguish targets at the same range with different velocities. Considering that the radar transmits a chirp signal every 0.5ms, if we assume that each target is moving at a constant velocity at the range of  $r_0$  over a period of time (e.g.  $N_d * T_c$ ), we can use the phase difference between adjacent bins in the time dimension at the same range of  $r_0$  to calculate the Doppler velocity. In this way, if there exists multiple targets with different velocities at the same range, we can obtain each target's velocity.

As discussed in Section 4.1.2, even a small change in the distance from the target at the range of  $r_0$  to the receiving antenna will induce a phase shift in the corresponding bin at  $r_0$  in the  $RP$ . Given the assumption that the target maintains a constant velocity over  $N_d * T_c$  time, the phase of the bins at  $r_0$  changes consistently throughout this interval. Then, according to [23], by performing an FFT (which is called Doppler FFT) on the bins at  $r_0$  over  $N_d * T_c$  time, each peak in the Doppler FFT result can represent a target moving at a specific velocity at the range of  $r_0$ . If we perform Doppler FFT on all ranges of  $RP$ , we are able to obtain the range doppler profile  $RDP(r, d, t)$ , where  $\text{abs}(RDP(r_0, d_0, t_0))$  represents the energy amplitude reflected by the target at the time of  $\frac{t_0}{N_c}$ , the range of  $\frac{r_0 c}{2B}$ , and the speed of  $\frac{d_0 c}{2T_c N_d f_c}$ .

Because of the low range resolution, the subtle features of gait pattern can't be displayed stably in the range-Doppler profile. Therefore, it is necessary to extract gait features based on Doppler information, which is why we compress the range dimension and transform the range-Doppler profile into the Doppler domain to calculate the micro-Doppler profile  $MDP(d, t)$ :

$$MDP(d, t) = \sum_{r=1}^{N_c} \text{abs}(RDP(r, d, t)) \quad (4)$$

**4.1.4 Extract Continuous Walking Stage.** During the actual data collection process, the patients are instructed to walk back and forth in front of the radar following the marked line on the ground. The whole walking process is shown as Figure 4(a), and its micro-Doppler profile is shown as Figure 4(b).

Based on the  $MDP$ , we categorize the walking process into four stages: starting stage, continuous walking stage, turning stage, and ending stage. Our system mainly focuses on the patient's continuous walking stage, where the majority of gait features are contained. Although start hesitation is a common symptom for PD patients, the starting stage hasn't been taken into consideration in this paper. Because PD patients are mostly elderly people, their reaction time after hearing the "start walking" command cannot be ignored. This makes it hard to accurately calculate the time from having the willingness to walk to actually starting walking.

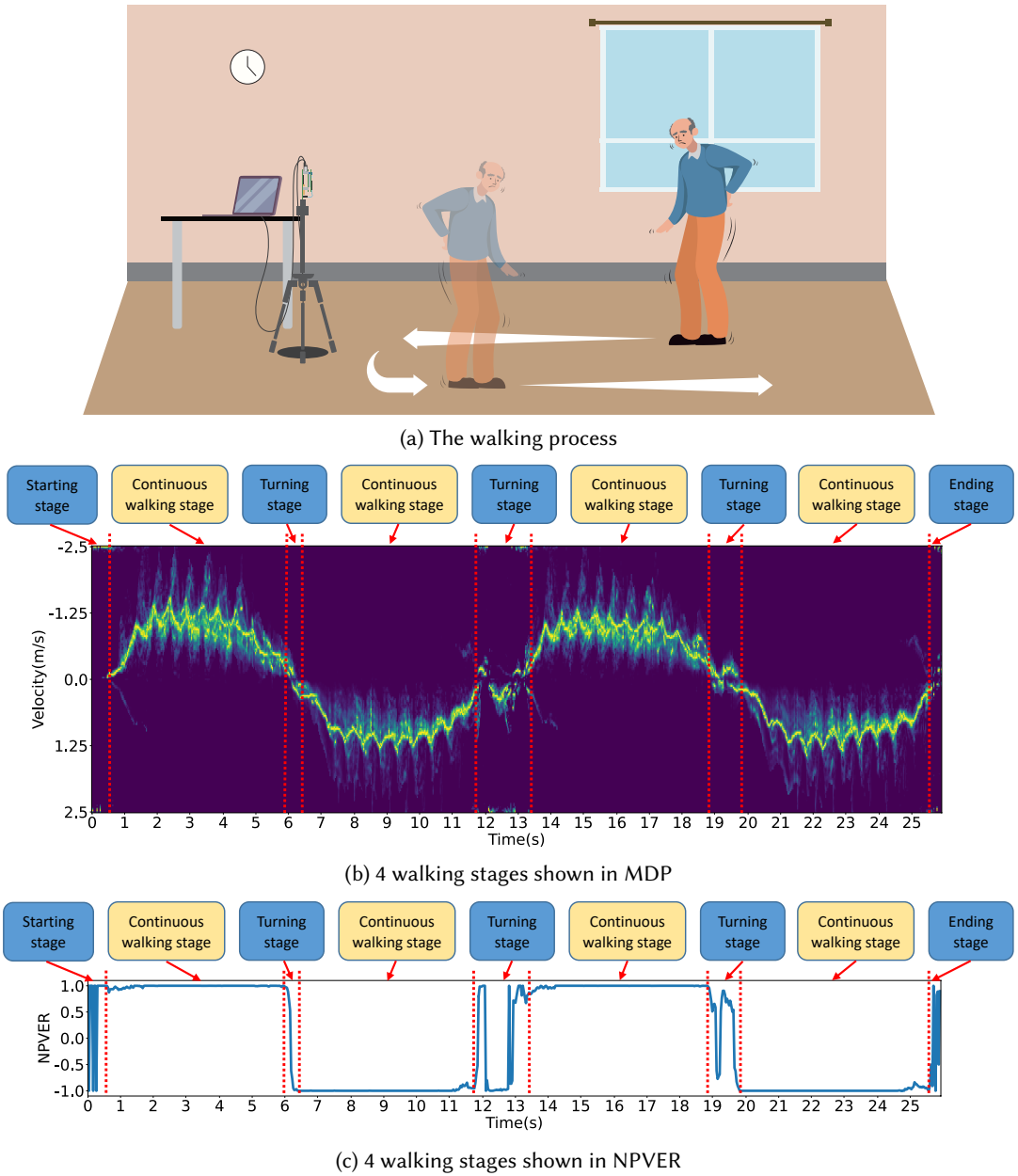


Fig. 4. Using NPVER to distinguish different stages during the walking process.

We propose the use of the Normalized Positive Velocity Energy Ratio (NPVER) to distinguish different walking stages. The NPVER is calculated as:

$$NPVER(t) = \sum_{d=\frac{1}{2}N_d}^{N_d} \frac{1}{0.5} (MDP(d, t) - 0.5) \quad (5)$$

The patient is standing still at both the starting stage and the ending stage, but even in the case of standing still, the patient's center-of-gravity and center-of-pressure may fluctuate over time [60]. This means that during these stages, the patient's body will move slightly back and forth. We can observe from Figure 4(c) that the NPVER will fluctuate around 0 at these two stages. During the continuous walking stage, the patient will keep walking towards or away from the radar. Because people often swing their arms while walking, arm movement in the opposite direction of the patient's forward motion introduces additional velocity components on the *MDP* when the arm swings backward. This will cause NPVER to fluctuate close to 1 or -1 (decided by the moving direction). During the turning stage, the patient will turn 180 degrees at the end of the marked line. In this stage, parts of the patient's body will get close to the radar while other parts will get away from the radar. Therefore, a change from 1 to -1, or from -1 to 1 with variation can be observed from the NPVER.

According to our observation, the continuous walking stage has a stable NPVER while all other stages exhibit time-varying NPVERs. Based on [59], the walking speed value of most people is 1.42m/s. Given that all participants in our dataset were asked to walk a 5m distance for 4 times and they were all PD patients with gait impairment or elderly people, we believe that their continuous walking stage time is beyond 2 seconds. This assumption allows us to design a stage extraction algorithm to extract the continuous walking stage we need. The algorithm will search the whole NPVER of the walking process to find the stage where the NPVER is greater than the predefined stability threshold and lasts longer than 2 seconds. The details of the algorithm are presented in Algorithm 1.

---

**Algorithm 1** Stage-Extraction Algorithm
 

---

**Input:** The normalized positive velocity energy ratio  $NPVER(x)$ , the stability threshold  $t$ , the number of received chirps per second  $n_c$ , the number of samples in  $NPVER(x)$   $n_s$

**Output:** The list  $C$  of the continuous walking stage's start time and end time.

```

1: Initialize the list C
2:  $x \leftarrow 1, s \leftarrow 0, e \leftarrow 0;$ 
3: while  $x < n_s$  do
4:   if  $NPVER(x) \times NPVER(x + 1) \leq 0$  or  $|NPVER(x)| < t$  then
5:     if  $(e - s) > 2 \times n_c$  then
6:       Put  $(s, e)$  to  $C$ ;
7:     else
8:        $s \leftarrow x, e \leftarrow s;$ 
9:     end if
10:   else
11:      $e \leftarrow e + 1;$ 
12:   end if
13: end while

```

---

## 4.2 Feature Extraction

**4.2.1 Segmentation of Disordered Gait.** In order to describe the temporal changes in gait features such as step duration and stride length, it is necessary to segment the entire walking process to obtain the start and end times of each step. Previous work usually uses the percentile method designed for Doppler radar which is defined as:

$$P(d, t) = \frac{\sum_0^d MDP(d, t)}{\sum_0^{d_{max}} MDP(d, t)} \quad (6)$$

where  $P(d, t)$  is the cumulated percentage of energy for frequencies lower than  $d$  at time  $t$  of the MDP [57]. With the threshold  $T_{torso}$ , the torso movement speed is estimated through the lowest frequency values which satisfy  $P(d, t) < T_{torso}$ , and the leg speed can be calculated through a different threshold  $T_{leg}$  as well. According to existing work, the  $T_{torso}$  is empirically set to 0.5 while  $T_{leg}$  is set to 0.9 [53].

The percentile-based method is effective for normal people but encounters limitations with PD patients who frequently exhibit gait impairments including leg dragging. The gait impairment leads to a lack of coordination between legs and arms for PD patients, while the arms' swinging speed trend is the same as that of the legs for normal people [62]. In this case, for PD patients, the arm speed may be at the maximum value when the leg speed is close to 0. Consequently, the speed curve extracted through the threshold  $T_{leg}$  may incorrectly attribute the velocity associated with arm movements to leg movements. If the extracted speed cannot correctly reflect the change in leg speed, the utilization of such speed for step segmentation would lead to incorrect results.

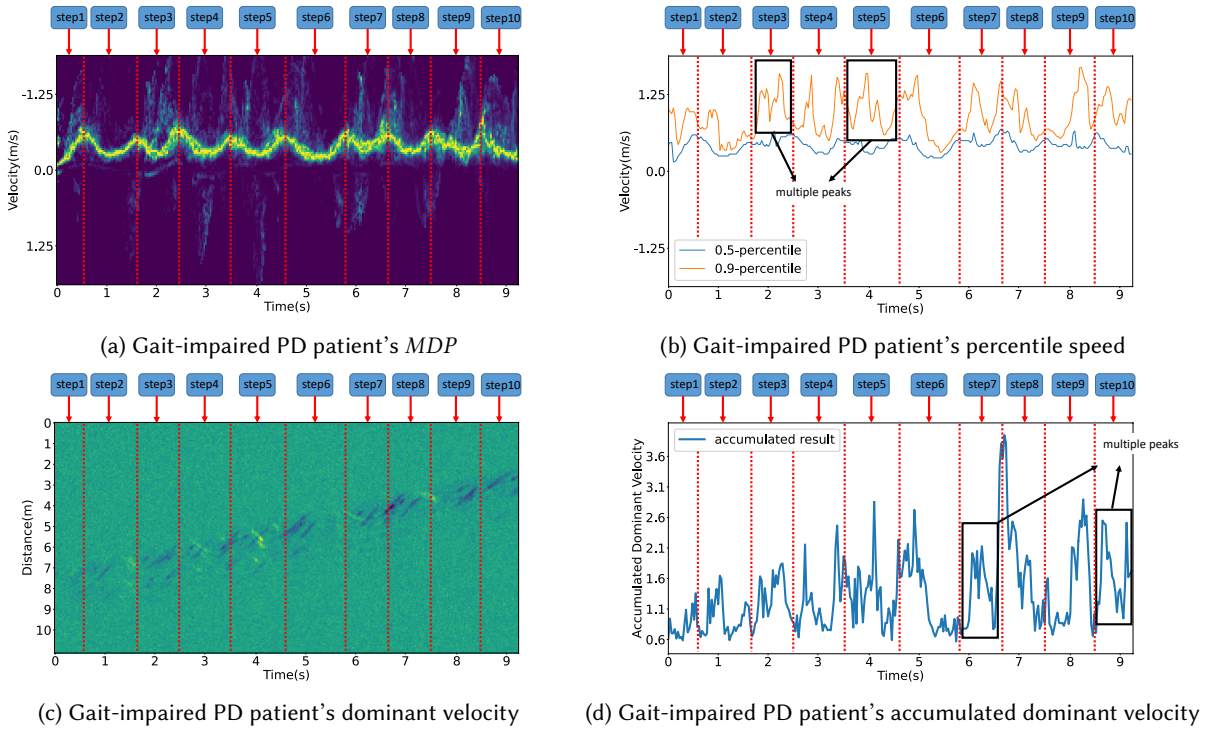


Fig. 5. Previous methods applied on PD patients with impaired coordination between arms and legs.

Figure 5(a) illustrates the MDP of a PD patient with impaired coordination between arms and legs. Further, Figure 5(b) demonstrates how arm speed influences leg speed, evidenced by the presence of multiple peaks in 0.9 percentile curve (which is regarded as leg speed) within single step cycles instead of a singular peak. This makes the leg speed cycles of PD patients unsuitable for step segmentation. The torso speed, which exhibits greater reflected energy, aligns consistently with the overall walking pattern. However, its amplitude is significantly lower in comparison to that of the arms and legs. Given the reduced range of motion observed in PD patients, attributed to their slower walking pace and shorter stride lengths, utilizing torso speed for step segmentation, as shown in Figure 6(a) and Figure 6(b), is not a reliable method as well (in some step cycles, there appear no peak in torso speed).

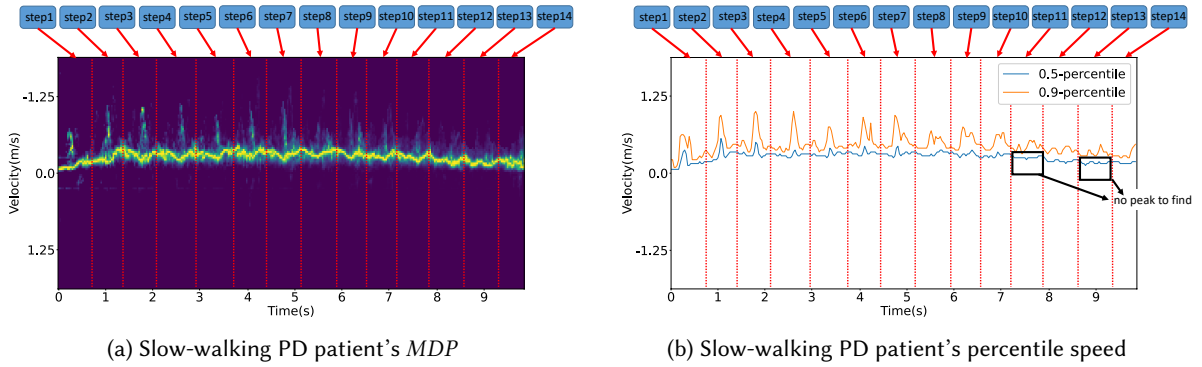


Fig. 6. Previous methods applied on PD patients with slow walking.

In addition to the percentile-based method, there is another method using compressed range-velocity data to get the dominant velocity  $\hat{V}$  to represent the user's lower limb velocity [65]. It can be calculated as follows:

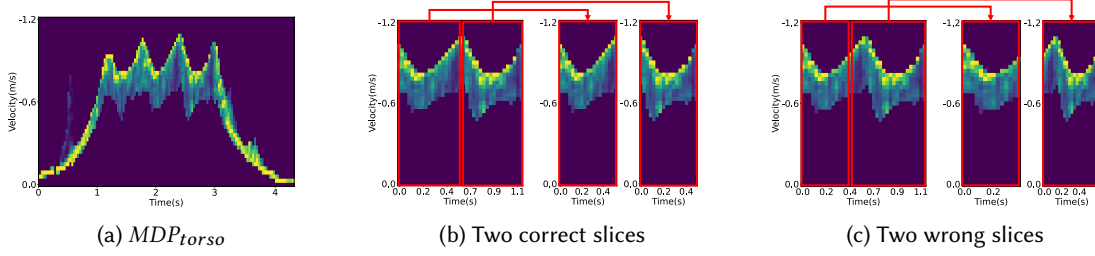
$$\hat{V}(r, t) = \frac{\sum_{d=1}^{N_d} (RDP(r, d, t) * d)}{N_d} \quad (7)$$

Upon obtaining the matrix  $\hat{V}$  representing the dominant velocity, the accumulated dominant velocity is calculated to observe temporal changes and the peak value identified from the accumulated dominant velocity corresponds to the step center, thus the gait segmentation can be done [65]. This method is also primarily effective for normal people because the disordered gait patterns typical of PD patients result in merged and indistinguishable peaks in the accumulated dominant velocity. This phenomenon is illustrated in Figure 5(d), where multiple peaks are evident within a single step cycle in the accumulated dominant velocity profile.

The aforementioned results indicate that relying solely on the velocity extracted from the *MDP* cannot effectively segment the steps. Despite the challenges caused by PD patients' uncoordinated limbs, slow gait, and short stride lengths, periodic changes in each step can still be observed in the *MDP*. Inspired by the way we observe the *MDP*, we find that we didn't solely use changes in the contour curve (which represents the speed extracted using percentile) to segment the steps. Instead, we make a judgment based on the similarity between two slices of *MDP* under a certain contour curve. Given that the leg speed can be influenced by the uncoordinated arm swinging speed, we choose to extract the  $MDP_{torso}$ , which represents the torso's speed pattern from the *MDP*, for more accurate segmentation:

$$MDP_{torso}(d, t) = \begin{cases} MDP(d, t) & \text{if } P(d, t) < T_{torso} \\ 0 & \text{if } P(d, t) > T_{torso} \end{cases} \quad (8)$$

With  $MDP_{torso}$  shown in Figure 7(a), we design a gait pattern match algorithm to quantify the similarity between two slices of  $MDP_{torso}$ . Since  $MDP_{torso}$  is a two-dimensional matrix, we utilize the cross-correlation coefficient to assess the similarity between two matrices. However, as shown in Figure 7(b), analysis of  $MDP_{torso}$  slices from two adjacent steps reveals the following differences: 1). The patients naturally accelerate and then decelerate during the walking process, so even two adjacent steps will have different speed patterns with the same changing trend. 2). Due to the impairment of balance and disordered gait in PD patients, the stride length and step duration are inconsistent between two adjacent steps. With these differences, the direct calculation of the cross-correlation coefficient of two  $MDP_{torso}$  slices cannot accurately represent the similarity in gait pattern.

Fig. 7. The  $MDP_{torso}$  and the gait slices.

The two correctly segmented  $MDP_{torso}$  slices input into our gait pattern matching algorithm exhibit similar overall gait pattern trends but differ in specific details (e.g. step duration, start speed, max speed, end speed), while two wrongly segmented  $MDP_{torso}$  slices have both different gait pattern trend and details (as shown in Figure 7(c)). To accurately quantify gait pattern similarity, our algorithm aims to mitigate the influence of the above details without changing the gait pattern trend. So we adjust the details in one slice to match those in another. As it is impossible to know how much the details of the two input slices are different, we consider one of the slices to be the reference slice and then enumerate all possible detail changes for the other. Since one of the slices we enumerate will have the same details as the reference slice, they will have the largest cross-correlation coefficient which is defined as the Gait Pattern Match Rate (GPMR). The detail changes to apply are as follows: 1). For the step duration difference, we stretch or compress the time dimension of the raw candidate slice to that of the reference slice (shown as Figure 8(a)) so that the candidate slice with the same time duration can be got (shown as Figure 8(b)). 2). For the max speed difference (shown as Figure 9), we stretch and compress the Doppler dimension to a certain extent to cover the reference slice max speed. 3). For the relative end speed difference (shown as Figure 10), We only care about the relative change between end speed and start speed, so shifts are applied with a certain slope.

It is important to clarify that the gait pattern match algorithm assigns a high GPMR not only to two slices with correct step segmentation, but also to any two slices that exhibit similar gait pattern trends. For example, consider two slices representing the 20% to 70% segment of their respective cycle times. Even though these two slices

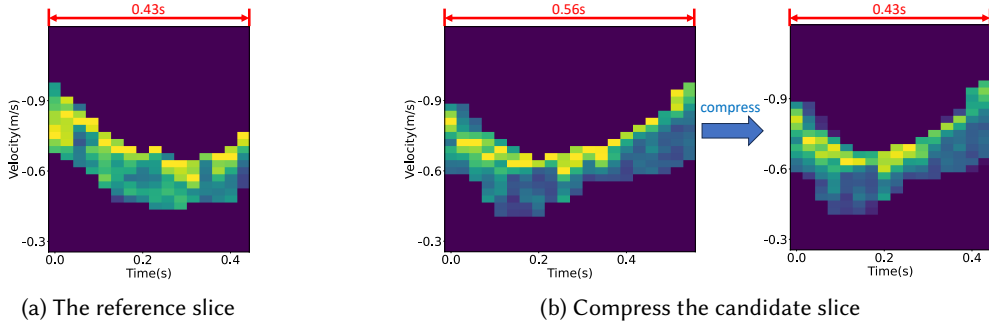


Fig. 8. Match the candidate slice time dimension to the reference slice through compression.

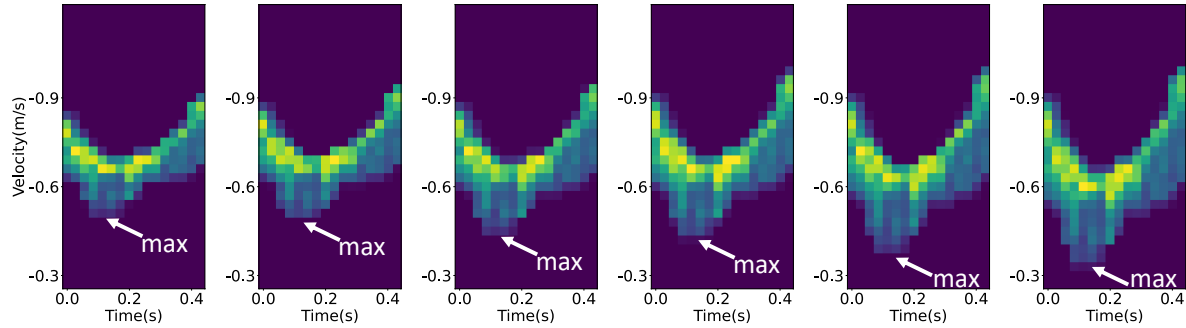


Fig. 9. The candidate slice with different max speeds.

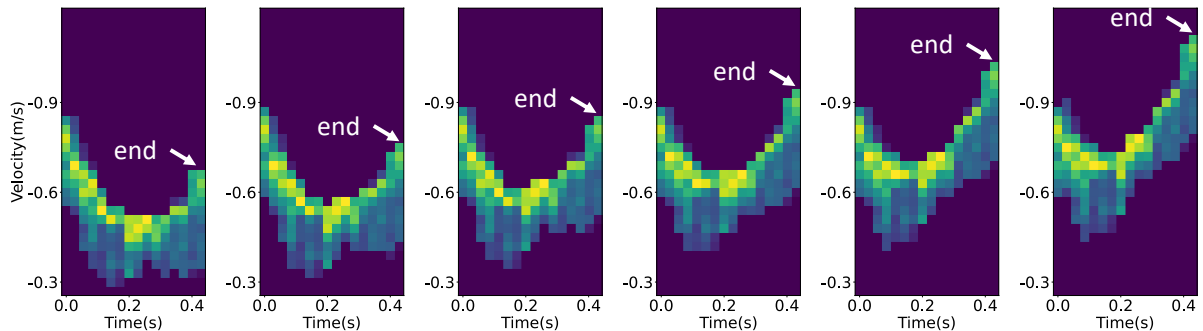


Fig. 10. The candidate slice with different end speeds.

correspond to different steps, our algorithm will assign a high GPMR because they cover equivalent portions of their cycles, resulting in the same gait pattern trend.

We introduce a gait segmentation algorithm based on the above gait pattern match algorithm. First, the percentile-based method is employed to extract the leg speed curve. Despite the fact that we can't correctly segment steps with the leg speed, the main frequency of the leg speed can be obtained through time-frequency analysis, which provides a reference step duration  $T_r$ . Subsequently, the gait segmentation algorithm is applied to the  $MDP_{torso}$  of the continuous walking stage. In this stage, the patient continues to walk without stopping (at least in the data we collected, no PD patients stop uncontrollably during walking), which means the patient starts the next step immediately after completing a step. We consider the current segmented step duration in the range from  $T_{cur}^{min}$  to  $T_{cur}^{max}$  ( $T_{cur}^{min} < T_r < T_{cur}^{max}$ ). We evaluated the accuracy of step duration segmentation for  $T_{cur}^{min} = 0.5T_r$ ,  $0.6T_r$ ,  $0.7T_r$ ,  $0.8T_r$ , as well as  $T_{cur}^{max} = 1.3T_r$ ,  $1.5T_r$ ,  $1.7T_r$ ,  $1.9T_r$ . We found that the best step duration segmentation accuracy was achieved when  $T_{cur}^{min} = 0.7T_r$  and  $T_{cur}^{max} = 1.5T_r$ . By enumerating all possible step durations from the above range and comparing the GPMR, we are able to find the best-segmented step duration  $T_{cur}^{best}$ . The details of the algorithm are presented in Algorithm 2.

**4.2.2 Calculation of Primary Features.** By applying the gait segmentation algorithm, we have already obtained the step duration, step start time, and step end time of each step in the whole walking process. Then, in order to calculate the stride length, it is necessary to determine the patient's position at each moment. By measuring the range at the step start time and at the step end time, we can accurately calculate the stride length for each step.

**Algorithm 2** Step-Segmentation Algorithm

**Input:** The previous step duration  $T_p$ , the continuous walking stage's  $MDP_{torso}$ , the reference step duration  $T_r$ , the current step start time  $t_s$ .

**Output:** The best segmented step duration  $T_{cur}^{best}$ .

---

```

1:  $T_{cur}^{best} \leftarrow T_r * 0.7;$ 
2:  $GPMR_{max} \leftarrow 0;$ 
3: while  $T_{cur} < T_r * 1.5$  do
4:    $MDP_{torso}^{cur} \leftarrow MDP_{torso}(t_s : t_s + T_{cur});$ 
5:    $T_n \leftarrow T_r * 0.7;$ 
6:   while  $T_n < T_r * 1.5$  do
7:      $MDP_{torso}^{next} \leftarrow MDP_{torso}(t_s + T_{cur} : t_s + T_{cur} + T_n);$ 
8:      $GPMR_c \leftarrow 0;$ 
9:     if  $T_p \neq 0$  then
10:       $MDP_{torso}^{pre} \leftarrow MDP_{torso}(t_s - T_p : t_s);$ 
11:       $GPMR_c \leftarrow GPMR(MDP_{torso}^{pre}, MDP_{torso}^{cur});$ 
12:    end if
13:     $GPMR_c \leftarrow GPMR_c + GPMR(MDP_{torso}^{cur}, MDP_{torso}^{next});$ 
14:    if  $GPMR_{max} < GPMR_c$  then
15:       $GPMR_{max} \leftarrow GPMR_c;$ 
16:       $T_{cur}^{best} \leftarrow T_{cur};$ 
17:    end if
18:     $T_n \leftarrow T_n + 1;$ 
19:  end while
20:   $T_{cur} \leftarrow T_{cur} + 1;$ 
21: end while

```

---

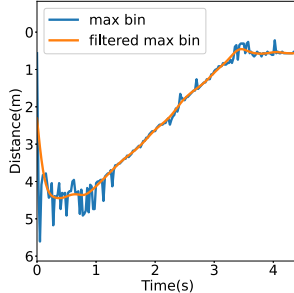
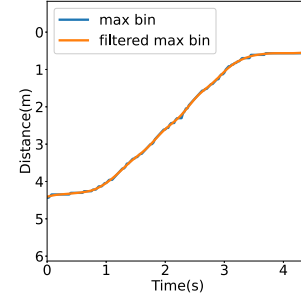
(a) The max bin extracted from the  $RP$ (b) The max bin extracted from the  $RP_{com}$ 

Fig. 11. Tracking the position of the patient.

Typically, a moving object at a certain position will generate a peak on  $RP$ , so that the position can be calculated by identifying the index of the bin with the highest energy. However, walking is a complex movement completed by the legs, knees, hips, torso, arms and other body parts. The bin with the highest energy at each time may not consistently correspond to the same body part, such as the torso or legs, leading to significant fluctuations in the calculated distances. Despite the application of Hampel and Butterworth filters, obtaining a smooth and regular position change curve remains challenging, as shown in Figure 11(a). Consequently, relying solely on  $RP$ -based position information to determine stride length is not advisable.

Given that relying solely on the amplitude (energy intensity) of the  $RP$  for object localization lacks stability and the range phase difference profile  $RP_{\Delta\varphi}$  can provide supplementary range information, we normalize both  $RP$  and  $RP_{\Delta\varphi}$ , then combine them to form the composite range profile  $RP_{com}$ , as described below:

$$RP_{com}(d, t) = \text{Normalized}(RP(d, t)) + \text{Normalized}(RP_{\Delta\varphi}(d, t)) \quad (9)$$

Then identify the bin with the highest energy in  $RP_{com}$  as the position of the patient. Following the filtering process, the patient's positional changes over time are acquired (refer to Figure 11(b)). Subsequently, the stride length is calculated using the positions recorded at the step start and end times. The gait velocity is then calculated by dividing the stride length by the step duration. We further calculate the time taken to walk per meter and the steps required to walk per meter with the features above as well.

**4.2.3 Calculation of Extended Features.** As mentioned in Section 4.2.1, PD patients have incoordination problems with their arms and legs, the speed curve extracted by the percentile-based method cannot correctly reflect the speed of the arms and legs.

However, an analysis of the  $MDP$  percentile matrix heatmap (shown as Figure 12) reveals that the velocity does not uniformly increase with the percentile. Furthermore, specific slices are extracted from the  $MDP$  percentile heatmap at predetermined intervals, and these slices are subsequently unwrapped to generate a 2D representation correlating speed with percentile. In the left slice (slice 1), the velocity slowly increases from the 0 to 0.55 percentile, followed by a rapid increase from the 0.55 to 1 percentile. In the right slice (slice 2), the velocity slowly increases from the 0.3 to 0.8 percentile range, whereas it exhibits rapid changes at other percentiles.

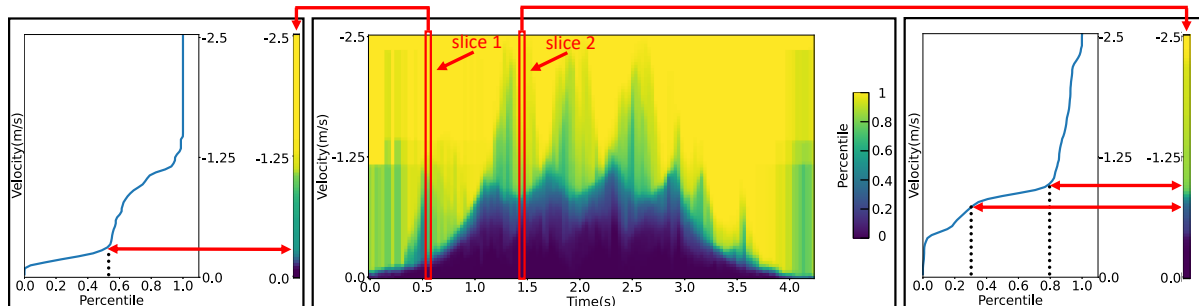


Fig. 12. The middle part contains the heatmap of a  $MDP$  percentile matrix and the color bar (the depth of color representing the value of the percentile), while the left and right parts show two slices extracted from the  $MDP$  percentile heatmap at specific intervals, and the 2D representation correlating velocity with percentile unwrapped from the slices.

We therefore extract the speed curves where their corresponding percentiles are 0.3, 0.55, and 0.8. For these curves, we only know they represent the speed changes of certain parts of the patient's body. While they may have real physical meanings, exploring these is not the focus of our paper. Similar to the previous method, we need to calculate both the moving range and speed. Given the absence of an  $RP$  for these speed curves, the moving range must be calculated by cumulating the speeds over their respective step durations. Also the moving speed can be obtained by dividing the moving range by step duration.

#### 4.3 Gait Impairment Assessment

The goal of mP-Gait is to use the obtained gait features to predict the gait score in UPDRS-III which can reflect the level of gait impairment of PD patients. Within the UPDRS-III gait assessment, gait impairment is categorized

into five grades, ranging from 0 to 4, where a higher score indicates more severe impairment. Since patients with scores above 2 require assistive devices for walking, such as walking sticks or walkers [42], and identifying the early-stage PD patients is more valuable, we primarily focus on the patients with scores ranging from 0 to 2. Therefore, the prediction task is defined as a 0 to 2 regression task.

We evaluated the performance of difference machine learning models on the prediction task including the well-known deep learning architectures based on 2-D spectrograms like Vision Transformers [10] and other methods utilizing deep learning models like GaitCube [39] and MU-ID [65]. Despite efforts to enhance their performance through data augmentation and various hyperparameter adjustments, the deep learning models did not outperform our approach in the PD gait assessment task. We hypothesize that the main reason lies in the limited scale of training dataset, which leads to overfitting during the training process. The deep learning models, though powerful, have numerous parameters and acquire large datasets. Previous works based on deep learning generally utilize much larger datasets (e.g. GaitCube involves 50,000 gait instances, more than ten times the size of our dataset).

Following analysis and practical experimentation, as detailed in Section 5.2.3, XGboost [8] was selected as the preferred model. The reasons are as follows:

- XGboost performs better on the limited-scaled dataset. Deep neural networks, characterized by their extensive parameter sets, necessitate large-scale datasets for effective training. The limited size of our dataset can lead to significant overfitting issues.
- Training an XGboost model takes a short amount of time. Compared to XGboost, deep learning methods generally have larger model sizes and require a longer training time.
- XGboost is a CPU-based machine learning methods, which can provide rapid inference in real-world scenarios such as hospitals, quickly delivering results. In contrast, deep learning methods require either on-site deployment with GPU-equipped devices or the use of cloud platforms with GPU support, complicating their implementation.

As a result, We use the extracted gait features including those without real physical meanings and train an XGboost model. The performance was validated using a 10-fold cross-validation and the model was optimized by grid search. We also find the features that contribute most to the prediction using SHAP [33].

## 5 IMPLEMENTATION AND EVALUATION

### 5.1 Implementation

**5.1.1 Experiment Setup.** mP-Gait employs the TI IWR6843ISK-ODS to transmit radar signals, and the DCA1000EVM data acquisition board to collect raw signal data. They are both mounted on a tripod at a height of 1 meter. This 60 GHz mmWave radar is equipped with three transmitters and four receivers, and is configured to transmit FMCW signals with a bandwidth of 4 GHz. For each FMCW chirp, the ADC samples the data, resulting in a collection of 256 data points ( $N_r$ ) within each chirp cycle ( $T_c$ ), achieving a range resolution of 0.0375 meters. The chirp periodicity is set at 0.0005 seconds, enabling the transmission of 2000 chirps per second. Assuming the motion velocity remains constant over a duration of 0.08 seconds, we select a window size  $N_d = 160$ , resulting in a velocity resolution of 0.03125m/s.

**5.1.2 Dataset Annotation.** In this study, we collaborated with the geriatric neurology department of a hospital to establish the dataset and we have the IRB (Institutional Review Boards) approval. The mmWave radar data of the 144 participants were collected in various places such as the outpatient department, the meeting rooms, and the wards. In this task, participants were instructed one by one to walk towards the mmWave radar from a distance of five meters, turn around, and walk back to the starting point, repeating this process twice (walking from one end to the other is referred to as one pass, so there are four passes in total). Neurologists stood behind

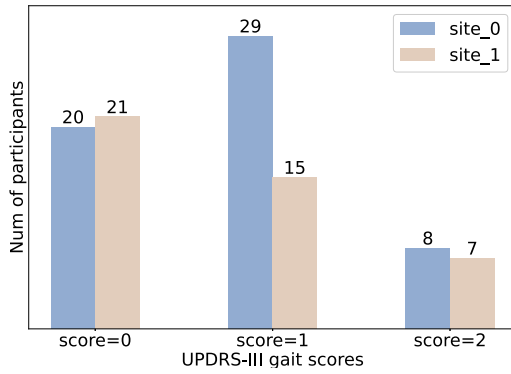


Fig. 13. The number of participants for each UPDRS-III gait impairment score in each site.

the radar to observe the participants' walking and assigned scores based on the gait assessment criteria in the UPDRS-III. We used these scores as labels for our subsequent regression analysis. The dataset comprised data from 123 PD patients and 21 healthy elderly control participants, with each of the 144 participants undergoing the gait data collection process only once. This means no matter whether the gait data collection for a certain participant was done at site0 or site1, that is the only gait data for that participant) and the UPDRS-III gait scores for each participant were calculated as the mean of the scores provided by three doctors. The distribution of the doctors' scores is shown in Figure 13 (it should be noted that some PD patients may only have hand tremors or other symptoms and do not show gait abnormalities. These patients are also scored as 0 points, which results in the number of patients scored as 0 points exceeds the number of health control participants).

**5.1.3 XGboost Regressor.** We trained an XGboost regression model to predict the UPDRS-III gait scores of participants. The features we extracted including stride\_length, 0.3\_percentile-length, 0.3\_percentile-speed, 0.55\_percentile-length, 0.55\_percentile-speed, 0.8\_percentile-length, 0.8\_percentile-speed, step\_duration, step\_per\_meter and time\_per\_meter are characterized as time-varying sequences. As we have already obtained the start and end times of each step for patients, we calculated the turning\_time representing the time cost for turning around. Whats more, we also calculated the mean and variance of NPVER within each step as step\_en\_ratio\_mean and step\_en\_ratio\_var. In this way, we got 13 kinds of sequence features.

Since each participant needed a different number of steps to finish the walking process, we opted to use the statistical features of these sequence features as the input instead of the sequences with different lengths. We calculated the minimum\_step, maximum\_step, average\_step, var\_step, and median\_step of the sequences as the statistical features. In addition, since PD patients may have the gait impairment of imbalance and bradykinesia especially when starting to walk, we took asymmetric\_ratio and first\_step into consideration. However, the angular resolution of mmWave radar is inadequate to distinguish whether the current step is left or right leg. Consequently, the asymmetric\_ratio calculated by dividing the mean of odd and even steps, only indicates the degree of imbalance of the participant, but cannot specify whether the impairment is in the left or right leg.

From above, we had 13 kinds of sequence features, and each sequence feature containing 7 statistical features across the 4 walking passes(except for turning\_time, the 7 statistical features only have 1 pass), so the input of the model was a vector with  $(12 * 4 + 1) * 7 = 343$  dimensions.

We used a greedy grid search algorithm with 10-fold cross-validation to find out the hyperparameters with the best performance in our XGboost model. In Table 2, we list the searching range for each hyperparameter and the optimal values.

Table 2. Best Hyperparameters and Search Ranges

Hyperparameters	Values	Ranges	Hyperparameters	Values	Ranges
learning_rate	0.05	[0.01, 1]	n_estimators	152	[1, 500]
max_depth	2	[1, 20]	min_child_weight	1	[1, 10]
gamma	0.05	[0, 0.6]	subsample	0.17	[0.01, 1]
colsample_bytree	0.33	[0.01, 1]	reg_alpha	1e-5	1e-5, 1e-2, 0.1, 1, 100
reg_lambda	1	1e-5, 1e-2, 0.1, 1, 100			

## 5.2 Evaluation

### 5.2.1 Accuracy of Primary Gait Feature Measurement.

**Experimental Goals:** We not only expect that the quantitative primary gait features extracted from the mmWave radar by mP-Gait can allow doctors to understand patients' gait patterns, but hope to use these features to estimate the patients' gait impairment severity as well. Therefore, we conducted an evaluation to assess the accuracy of these primary gait feature measurements. Since primary features like gait velocity and the time taken to walk per meter are calculated through stride length and step duration, we mainly focus on the accuracy of these two features.

**Evaluation Metrics:** Because primary gait features are continuously changing values, we use the mean absolute error (MAE) to measure the accuracy of the calculated stride length and step duration.

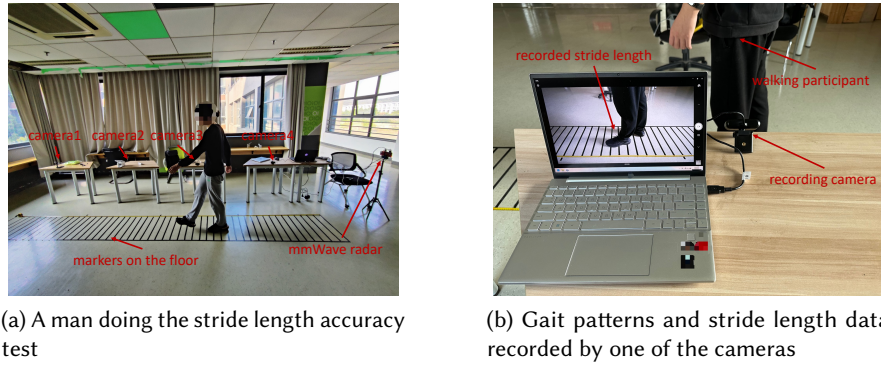


Fig. 14. The stride length accuracy evaluation and the camera data collected.

**Ground Truth:** 1. For step duration accuracy, we manually annotated MDP data of 100 participants (including 42 with UPDRS gait score of 0, 43 with UPDRS gait score of 1, and 15 with UPDRS gait score of 2) with the recorded videos provided by the hospital out of all 144 participants to establish the ground truth step duration information for each step. 2. For stride length accuracy, because setting up cameras in the hospital would infringe on patients' privacy which would make some of them uncomfortable, we set up a system in the laboratory as Figure 14(a). By deploying 4 cameras (each positioned as Figure 14(b)) and adding markers on the floor at 10 cm intervals, we were able to simultaneously record stride length while collecting mmWave gait data. In this way, we collected the ground truth stride length data from four male and one female participants, with heights ranging from 165cm to 180cm. Each participant was asked to walk back and forth following the lines as illustrated, repeating 3 times.

**Evaluation Results:** To evaluate step duration accuracy, we compared mP-Gait with the method using dominant velocity [65] and the method using percentile [57]. Since all PD patients with UPDRS gait score above 0 exhibit various degrees of gait impairments, including shuffling gait, festination, and lack of arm and leg coordination etc, these gait impairments led to decreased step duration accuracy for existing methods. Figure 15(a) demonstrates that mP-Gait has similar step duration accuracy for patients with UPDRS gait scores of 0 and 1 ( $MAE = 0.088s$  and  $MAE = 0.094s$  respectively). For patients with UPDRS gait score of 2, although our method's error increased slightly ( $MAE = 0.119s$ ), mP-Gait still outperformed the existing methods ( $MAE = 0.156s$  and  $MAE = 0.147s$  respectively), and even lower than existing methods' errors for patients with UPDRS gait score of 1 ( $MAE = 0.133s$  and  $MAE = 0.128s$  respectively). For stride length accuracy, the accuracy results for each participants are shown as Figure 15(b). We get a total stride length calculation  $MAE$  of  $7.63cm$ .

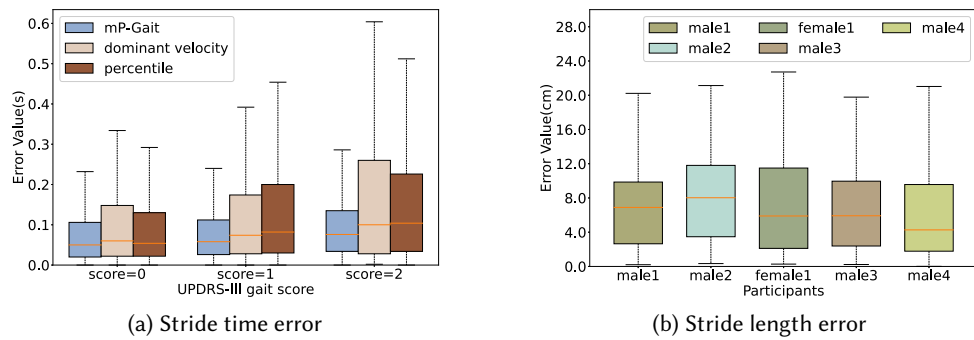


Fig. 15. The stride length error and the step duration error.

### 5.2.2 Accuracy of UPDRS-III Gait Score Prediction.

**Experimental Goals:** We expect that mP-Gait can utilize the extracted primary gait features and extended gait features to predict fine-grained UPDRS-III gait scores. Therefore, we train an XGboost model and evaluate its prediction accuracy, making sure that mP-Gait can assist doctors in assessing patients' gait impairment severity.

**Evaluation Metrics:** We train an XGboost regression model to obtain continuous fine-grained UPDRS-III gait scores, so we use  $MAE$  to measure the accuracy of our predictions.

**Ground Truth:** We used the gait data collected from two sites including 144 participants who could complete the walking test without extra assistance, and used the UPDRS-III gait scores (including 0 points, 1 points and 2 points) given by neurologists as the ground truth.

**Evaluation Results:** The XGboost model we have trained have strong generalizability. As mentioned in Section 5.1.2, regardless of whether the gait data collection for a certain patient was done at site0 or site1, that is the only gait data for that patient. That is to say, no matter how we split our dataset, there won't be gait data collected by the same person in both the training set and test set. This ensures that our model is person-independent. Furthermore, we trained the XGboost regression model using data from one site and employed data from another site for testing to demonstrate mP-Gait's independence from environmental factors such as lighting and room layouts. We calculated the  $MAE$  of the two models trained on different sites across various UPDRS-III gait scores, as illustrated in Figure 16(a), while Figure 16(b) details the distribution of these errors. Utilizing data from a single site leads to a relatively small number of patients, resulting in lower model accuracy compared to training on the dataset aggregated from all sites (training on all sites:  $MAE=0.379$ , training on site0:  $MAE=0.431$ , training on site1:  $MAE=0.386$ ). Despite this, our model demonstrates considerable accuracy.

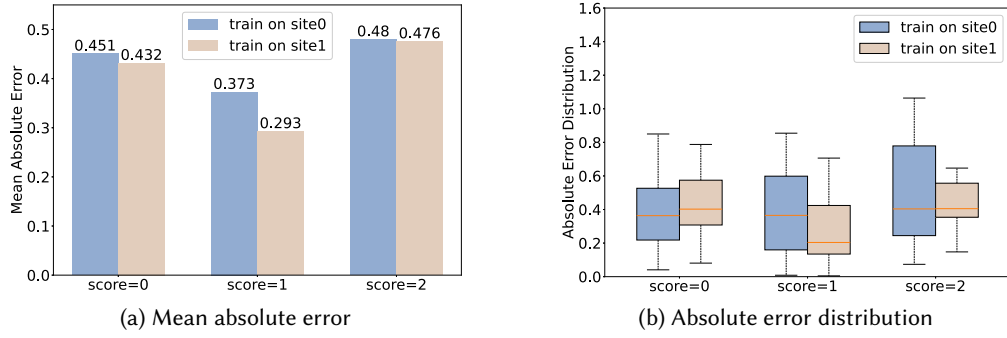


Fig. 16. The regression result of different UPDRS-III gait scores for mP-Gait in different sites.

### 5.2.3 Comparison with Deep-learning Methods and state-of-the-art Baseline Methods.

**Experimental Goals:** mP-Gait is first evaluated against two popular deep learning models. Given that deep learning methods necessitate fixed-size input matrices, the *MDP* spectrograms were segmented using a 1.4-second sliding window to generate the inputs for these models. The models evaluated include: 1. **CNN+LSTM**. This model utilizes CNNs to extract local features, while LSTMs to capture temporal information in the time series. The model contains 3 convolutional layers, and an LSTM layer with a hidden size of 512. This combination enables better understanding of spectral-temporal representations. 2. **ViT**. Vision Transformers [10] achieve outstanding performance in CV tasks. The *MDP* spectrogram treated as an image is firstly split into patches as the input. Learnable class token and absolute position encoding are used before the embeddings are input into the Transformer Encoder. Since the scale of our dataset is limited, we utilize a relatively small architecture, which shows better performance than deeper ones. The number of encoder layers is only 2 and the number of heads is 4. The hidden size is 128, while the embedding size is 384. What is more, the probability of dropout is set to 0.5 to avoid overfit.

In addition to the two previously discussed deep learning architectures, we also evaluate our approach against two state-of-the-art methods that focus on user identification via gait analysis using mmWave radar signals, which are the closest related works. These methods have been appropriately adapted to meet the specific requirements of PD gait assessment. Additionally, each of these methods has its specifically designed input matrices, so we use the inputs mentioned in the papers instead of the *MDP* spectrum to achieve the best performance. The methods evaluated include: 1. **MU-ID**: MU-ID utilizes compressed range-velocity data to extract the dominant velocity, subsequently segmenting the data by gait cycles. For each cycle, the Time-Range-Doppler map is generated and input into a regression network consisting of four convolutional layers respectively followed by a max pooling layer. 2. **GaitCube**: GaitCube tracks range bins associated with human motion and extracts the “gait data cube” (a novel 3-D joint-feature representation of micro-Doppler and micro-range signatures over time). This cube illustrates the dynamic relationships between time, frequency, and range, and is subsequently processed by a convolutional neural network composing 3 convolutional layers, two of which are followed by a pooling layer.

For the aforementioned four deep learning models, we all used a batch size of 128 to train for 50 epochs. Except for the Vision Transformer, which uses GELU as the activation function, all other models use ReLU.

**Evaluation Metrics:** All methods ultimately output regression results to predict the UPDRS-III gait scores, so we use MAE to evaluate the performance of different methods.

**Ground Truth:** We used the same gait dataset as Section 5.2.2 for all methods.

**Evaluation Results:** The performances of each method are shown as Table 3. It can be observed that using specifically designed input matrices shows better results compared to the MDP spectrum. However, due to the limited scale of our dataset, the deep learning methods perform no better than mP-Gait.

Table 3. Different Methods' Performances

Method	Input	MAE
mP-Gait (XGboost)	343-dimension features	0.379
CNN+LSTM	spectrograms	0.417
Vision Transformer	spectrograms	0.410
GaitCube	gait data cube	0.403
MU-ID	range-time-velocity map	0.409

#### 5.2.4 mP-Gait's Ability to Predict Fine-grained Scores.

**Experimental Goals:** The XGboost regression model that we trained can obtain a continuous gait score prediction, but whether this prediction score can represent the participant's fine-grained UPDRS-III gait score still needs evaluation. Considering a participant with an actual UPDRS-III gait score of 1.4 and the doctor gave a score of 1, if our model predicts a result of 0.7 or 1.3, the final absolute error will be 0.3 in both cases, but clearly 1.3 is the correct fine-grained score, while 0.7 is wrong.

**Evaluation Metrics:** We still utilize the MAE to assess the accuracy of the XGboost model's prediction results compared to the fine-grained ground truth UPDRS-III gait scores.

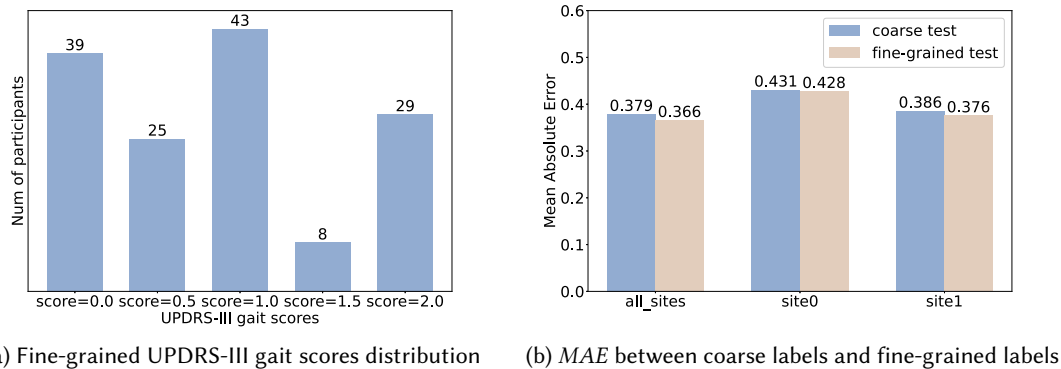


Fig. 17. The regression results of the XGboost model, which was trained using coarse labels, tested across different sites with both coarse and fine-grained labels.

**Ground Truth:** UPDRS-III gait scores must be strictly assigned according to the gait features outlined in Table 1 in order to ensure clinical meaning. Consequently, it is not possible to obtain fine-grained UPDRS-III gait scores with clinical meaning for each participant as ground truth labels. However, even neurological experts often face challenges in precisely scoring patients whose symptoms fall between standard UPDRS-III categories, such as between scores of 0 and 1 or 1 and 2. Accordingly, for patients whom experts felt difficult to assign the score precisely, we recorded them with intermediate scores of 0.5 and 1.5, although these scores do not have actual clinical meaning. In this way, we got our fine-grained ground truth UPDRS-III gait scores and the data distribution is shown as Figure 17(a).

**Evaluation Results:** The results are shown as Figure 17(b). It can be seen that for the XGboost regression model trained using coarse labels(UPDRS-III gait scores containing only 0, 1, 2) from all sites, when testing using coarse labels, the *MAE* is 0.379. However, if using fine-grained labels(UPDRS-III gait scores containing 0, 0.5, 1, 1.5, 2) for testing, the *MAE* decreases to 0.366. As experts can score most patients accurately, the decrease in *MAE* is small with only 33 patients having a score of 0.5 or 1.5. This decrease in *MAE* indicates that the results predicted by the XGboost regression model are closer to the patients' actual UPDRS-III gait scores compared to the coarse labels used for training. Consequently, this demonstrates that the XGboost regression model has the ability to predict fine-grained scores.

In order to further demonstrate mP-Gait's fine-grained UPDRS-III gait score prediction ability, we used the predicted score changes before and after medication to validate whether mP-Gait's predicted results can correctly reflect the patients' gait pattern response to medication in Section 6.

### 5.2.5 Analysis of the features' impact on prediction.

**Experimental Goals:** We have evaluated the predictive accuracy of the UPDRS-III gait scores using our XGboost model. We also expect to analyze the impact of the input features on the model, so that the effective features for assessing PD gait impairment severity can be found. Additionally, this analysis will allow us to find out whether the model accurately recognizes the relationships between these features and PD gait impairment severity.

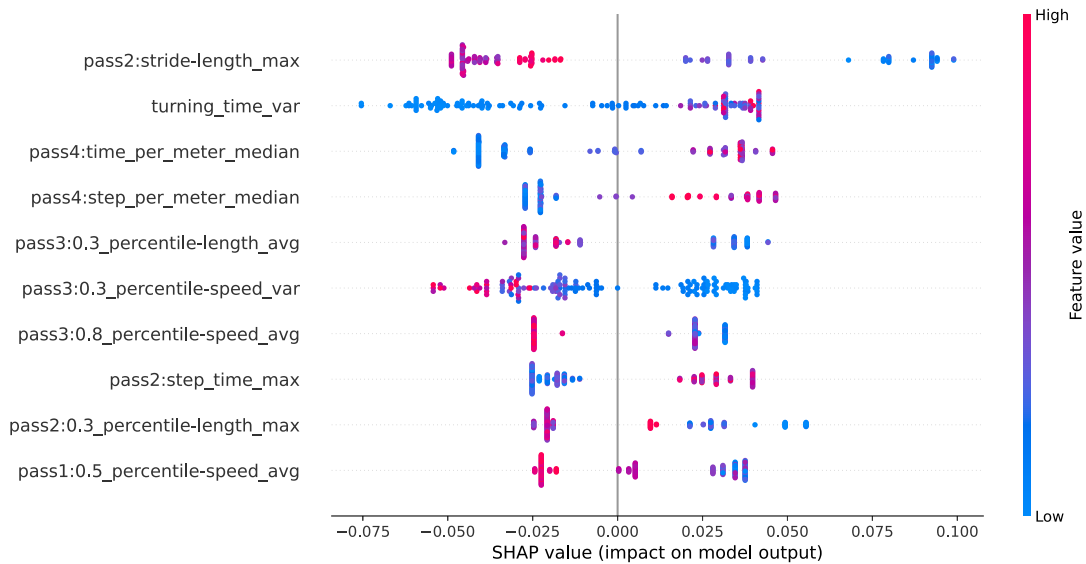


Fig. 18. The top 10 important features' impact calculated by SHAP.

**Evaluation Results:** We employed the SHAP framework [33] to quantify the impact of each feature on the model's predictions, as illustrated in Figure 18. Each point corresponds to the specific gait feature of one patient. The color of each point represents the feature's value: deeper blue indicates smaller values and deeper red indicates larger values. The position of each point along the x-axis demonstrates the influence of the feature on the prediction: points positioned to the right of the zero line suggest a positive impact (increasing the prediction), whereas those to the left indicate a negative impact (decreasing the prediction) [44].

Figure 18 shows that for the feature “stride-length\_max”, which reflects the maximum stride length of patients, larger values are associated with lower predicted UPDRS-III gait scores. This observation correlates with the clinical characteristic that PD patients generally exhibit reduced motion amplitudes; thus, a larger stride length suggests a lower UPDRS-III gait score, indicative of a condition closer to that of healthy people. Similarly, for “time\_per\_meter\_median”, which is the median time required to walk for one meter, larger values correspond to higher predicted UPDRS-III gait scores. This is consistent with the clinical observation that a longer time to walk a fixed distance is indicative of slower movements, which mean higher UPDRS-III gait scores in patients.

## 6 CASE STUDY

To further evaluate the performance of mP-Gait in real-world scenarios, we deployed mP-Gait in a completely new site, a hospital ward which was distinct from the previous clinic room (site0) and conference room (site1) mentioned in Section 5.1.2. Patients (not involved in the Section 5.1.2 dataset collection) were instructed one by one to walk back and forth twice between two ends, completing four passes in total (walking from one end to the other is referred to as one pass). Given that mP-Gait operates without the need for any wearable devices, each gait signal collection only took 1 – 3 minutes depending on the patient’s gait impairment severity. We repeated the gait signal collection process 6 times within one day for each patient and recorded the times of their medication intake as well. In this way, we can observe the changes in gait features of the same patient before and after taking medication within a day, as well as the changes in the fine-grained UPDRS-III gait score predicted by mP-Gait.

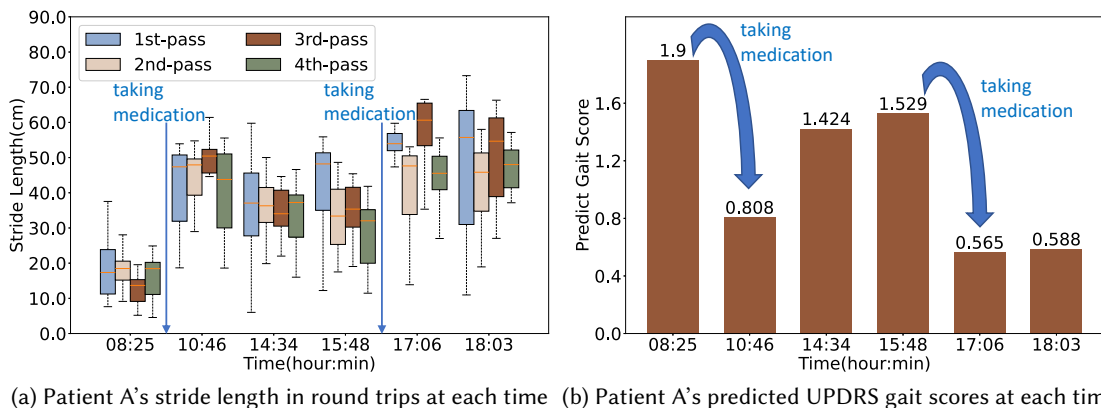


Fig. 19. Stride length variation in one day for the patient completing the same two round trips and the predicted UPDRS-III gait scores using our XGboost regression model with the gait features.

Through the analysis of gait signals, we obtained patient A’s stride length distribution for each pass collected at different times within one day (as shown in Figure 19(a)) and the UPDRS-III gait scores predicted by our XGboost regression model trained with the dataset discussed in Section 5.1.2 (as shown in Figure 19(b)). The precise extraction of gait features allows the UPDRS-III gait scores predicted by mP-Gait to not only accurately reflect significant improvements in gait condition after taking medication but also to illustrate the deterioration in gait condition as medication efficacy wanes over time. As illustrated in Figure 19(a), at 8:25 am, after a night without medication, patient A exhibited severely impaired gait with notably short stride lengths. Consequently, in Figure 19(b), we can see that the predicted UPDRS-III gait score was also the highest at 1.9. After signal collection, patient A took medication, and no additional doses were taken from 10:46 am to 15:48 pm. Observations revealed

that by 10:46 am, the stride length was much higher than that at 8:25 am but progressively declined until 15:48 pm. Correspondingly, the predicted UPDRS-III gait scores increased from 0.808 to 1.529 over the period, reflecting this change. Then patient A took medication again, and from 17:06 pm to 18:03 pm, the stride length increased again with UPDRS-III gait scores decreasing at the same time.

These accurate and fine-grained scores enable doctors to quantify medication effects in different patients so that the dosages and types of medication can be rationally adjusted to avoid dopamine peaks and other side effects.

## 7 DISCUSSION

**Limitations of the dataset:** Unlike vision-based methods being able to use existing recording videos of PD patients' UPDRS examinations with scores [14] as the dataset, our method faced challenges in rapidly collecting extensive radar gait data. Consequently, this limitation led to an imbalanced number of samples with different scores in our dataset. However, our evaluation demonstrated mmWave radar's sensing capability in extracting gait features and predicting UPDRS-III gait scores. These features and scores can effectively capture changes in a patient's gait impairment severity before and after medication, even in a new site with a new patient. We believe that with the widespread of mmWave-based sensing, a larger labeled PD patients' gait dataset will become available and mP-Gait will show better performance in gait score prediction.

**Extracting turning stages:** We identified the starting, continuous walking, turning, and ending stages of walking by analyzing the Normalized Positive Velocity Energy Ratio (*NPVER*). However, in actual experiments, we found this method couldn't cover all the turning stage patterns. Specifically, when patients reached the end, there were two patterns of turning: 1.The patient stopped walking, turned around, and walked again. 2.The patient walked to turn 180° without a clear stop. mP-Gait effectively extracted the first turning pattern. However, the second pattern, where patients simultaneously walk forward and turn, complicates the identification of the turning stage's start and end points. To avoid this, we required patients to use the first turning pattern during data collection. This did add discomfort during walking, and we will explore more precise methods for the second turning pattern in future work.

**Not using skeleton-based approaches:** Vision-based wireless gait analysis methods typically extract the 3D body mesh and the skeletons from video first and then analyze the joint motions for predicting gait impairment severity [13, 32]. mmWave radar showed a similar potential [41], but we believe the skeleton extraction process already introduces errors. Using gait features with error for further analysis cannot achieve the same high prediction accuracy as 3D motion capture which can directly obtain the skeletons. (Video-based skeleton extraction usually has less than 85% gait impairment severity prediction accuracy [13, 35, 44], while 3D motion capture system has over 95% [3]). In this case, we did not use point clouds-based methods to obtain the skeleton before gait analysis.

**Data collection in daily life:** Although mP-Gait collects gait data easily, we still required patients to walk back and forth between fixed endpoints. Our stride length calculation relied on linear distances between the patient and radar, so mP-Gait cannot work when the patients are freely walking around in a room with many obstacles. While COTS mmWave radars have antenna arrays, we did consider using the angle-FFT-based methods [61, 65] to extract gait features by calculating the changes in the patient's orientation. However, as the UPDRS-III gait score can only be scored based on the patient's gait data when walking in a straight line, doctors have no way to assign medically meaningful scores based on the patient's freely walking gait features (which include a lot of unpredictable acceleration, deceleration, and turning). This makes it difficult to evaluate, so we leave more unobtrusive data collection as our future work.

## 8 CONCLUSIONS

We first introduced mP-Gait, a Parkinson's Disease (PD) gait analysis system which utilizes COTS mmWave radar to sense walking motions. We first designed a gait segmentation algorithm robust to gait disorder, leveraging a 2D micro-Doppler profile matching algorithm to analyze each step of PD patients' walking process. Second, we designed an algorithm combining the micro-Doppler profile and range profile to calculate the primary gait features like stride length and step duration for each segmented step. We also extracted extended percentile gait features based on the patterns of the micro-Doppler profile. Then, we collected gait data from 144 participants with different UPDRS-III scores in two sites and trained an XGboost regression model. Next, by obtaining gait features, we predicted PD patients' UPDRS-III gait scores. Finally, the evaluation results demonstrated that mP-Gait achieved mean absolute errors of 7.63cm and 0.096s for stride length and step duration calculation respectively, and achieved  $MAE=0.379$  in predicting UPDRS-III gait scores. We believe that this work demonstrated the potential of mP-Gait for PD gait analysis and made unobtrusive daily PD monitoring possible.

## ACKNOWLEDGMENTS

This work was supported in part by the National Natural Science Foundation of China under Grant U22A2031, 62272223, 62272213, 82101332, 62102006.

## REFERENCES

- [1] Libak Abou, Joseph Peters, Ellyce Wong, Rebecca Akers, Mauricette Sènan Dossou, Jacob J Sosnoff, and Laura A Rice. 2021. Gait and balance assessments using smartphone applications in Parkinson's disease: a systematic review. *Journal of medical systems* 45 (2021), 1–20.
- [2] M Abroskina, V Ondar, S Ismailova, S Subocheva, A Khomchenkova, V Gurevich, S Kondratiev, E Mozheyko, and S Prokopenko. 2021. Video Analysis of Human Gait: Advantages and Disadvantages in Neurological Diagnostics. In *2021 International Symposium on Biomedical Engineering and Computational Biology*. 1–7.
- [3] Satyabrata Aich, Pyari Mohan Pradhan, Jinse Park, and Hee-Cheol Kim. 2018. A machine learning approach to distinguish Parkinson's disease (PD) patient's with shuffling gait from older adults based on gait signals using 3D motion analysis. *Int. J. Eng. Technol.* 7, 3.29 (2018), 153–156.
- [4] Mubarak A Alanazi, Abdullah K Alhazmi, Osama Alsattam, Kara Gnau, Meghan Brown, Shannon Thiel, Kurt Jackson, and Vamsy P Chodavarapu. 2022. Towards a low-cost solution for gait analysis using millimeter wave sensor and machine learning. *Sensors* 22, 15 (2022), 5470.
- [5] Sizhe An, Yigit Tuncel, Toygun Basaklar, Gokul K Krishnakumar, Ganapati Bhat, and Umit Y Ogras. 2021. Mgait: Model-based gait analysis using wearable bend and inertial sensors. *ACM Transactions on Internet of Things* 3, 1 (2021), 1–24.
- [6] MS Bryant, DH Rintala, JG Hou, EC Lai, and EJ Protas. 2011. Effects of levodopa on forward and backward gait patterns in persons with Parkinson's disease. *NeuroRehabilitation* 29, 3 (2011), 247–252.
- [7] Marianna Capecci, Lucia Pepa, Federica Verdini, and Maria Gabriella Ceravolo. 2016. A smartphone-based architecture to detect and quantify freezing of gait in Parkinson's disease. *Gait & posture* 50 (2016), 28–33.
- [8] Tianqi Chen and Carlos Guestrin. 2016. Xgboost: A scalable tree boosting system. In *Proceedings of the 22nd ACM SIGKDD international conference on knowledge discovery and data mining*. 785–794.
- [9] Taylor Chomiak, Wenbiao Xian, Zhong Pei, and Bin Hu. 2019. A novel single-sensor-based method for the detection of gait-cycle breakdown and freezing of gait in Parkinson's disease. *Journal of Neural Transmission* 126 (2019), 1029–1036.
- [10] Alexey Dosovitskiy, Lucas Beyer, Alexander Kolesnikov, Dirk Weissenborn, Xiaohua Zhai, Thomas Unterthiner, Mostafa Dehghani, Matthias Minderer, Georg Heigold, Sylvain Gelly, et al. 2020. An image is worth 16x16 words: Transformers for image recognition at scale. *arXiv preprint arXiv:2010.11929* (2020).
- [11] A Dural, MB Atay, C Akbstancı, and A Kucukdeveci. 2003. Impairment, disability, and life satisfaction in Parkinson's disease. *Disability and rehabilitation* 25, 7 (2003), 318–323.
- [12] Bekir Durmus, Ozlem Baysal, Sibel Altinayar, Zuhal Altay, Yuksel Ersoy, and Cemal Ozcan. 2010. Lower extremity isokinetic muscle strength in patients with Parkinson's disease. *Journal of Clinical Neuroscience* 17, 7 (2010), 893–896.
- [13] Mark Endo, Kathleen L Poston, Edith V Sullivan, Li Fei-Fei, Kilian M Pohl, and Ehsan Adeli. 2022. GaitForeMer: Self-Supervised Pre-Training of Transformers via Human Motion Forecasting for Few-Shot Gait Impairment Severity Estimation. In *Medical Image Computing and Computer Assisted Intervention—MICCAI 2022: 25th International Conference, Singapore, September 18–22, 2022, Proceedings, Part VIII*. Springer, 130–139.

- [14] M Kelley Erb, Daniel R Karlin, Bryan K Ho, Kevin C Thomas, Federico Parisi, Gloria P Vergara-Diaz, Jean-Francois Daneault, Paul W Wacnik, Hao Zhang, Tairmae Kangarloo, et al. 2020. mHealth and wearable technology should replace motor diaries to track motor fluctuations in Parkinson's disease. *NPJ digital medicine* 3, 1 (2020), 6.
- [15] Nir Giladi, Joseph Tal, Tali Azulay, Oliver Rascol, David J Brooks, Eldad Melamed, Wolfgang Oertel, Werner H Poewe, Fabrizio Stocchi, and Eduardo Tolosa. 2009. Validation of the freezing of gait questionnaire in patients with Parkinson's disease. *Movement disorders: official journal of the Movement Disorder Society* 24, 5 (2009), 655–661.
- [16] Yi Han, Xiangzhi Liu, Ning Zhang, Xiufeng Zhang, Bin Zhang, Shuoyu Wang, Tao Liu, and Jingang Yi. 2023. Automatic Assessments of Parkinsonian Gait with Wearable Sensors for Human Assistive Systems. *Sensors* 23, 4 (2023), 2104.
- [17] Naoya Hasegawa, Vrutangkumar V Shah, Patricia Carlson-Kuhta, John G Nutt, Fay B Horak, and Martina Mancini. 2019. How to select balance measures sensitive to Parkinson's disease from body-worn inertial sensors—separating the trees from the forest. *Sensors* 19, 15 (2019), 3320.
- [18] Jeffrey M Hausdorff, Merit E Cudkowicz, Renée Firtion, Jeanne Y Wei, and Ary L Goldberger. 1998. Gait variability and basal ganglia disorders: stride-to-stride variations of gait cycle timing in Parkinson's disease and Huntington's disease. *Movement disorders* 13, 3 (1998), 428–437.
- [19] Deborah Hirtz, David J Thurman, Katrina Gwinn-Hardy, M Mohamed, AR Chaudhuri, and R Zalutsky. 2007. How common are the “common” neurologic disorders? *Neurology* 68, 5 (2007), 326–337.
- [20] Margaret M Hoehn, Melvin D Yahr, et al. 1998. Parkinsonism: onset, progression, and mortality. *Neurology* 50, 2 (1998), 318–318.
- [21] Chen-Yu Hsu, Yuchen Liu, Zachary Kabelac, Rumen Hristov, Dina Katabi, and Christine Liu. 2017. Extracting gait velocity and stride length from surrounding radio signals. In *Proceedings of the 2017 CHI Conference on Human Factors in Computing Systems*. 2116–2126.
- [22] Sheau-Ling Huang, Ching-Lin Hsieh, Ruey-Meei Wu, Chun-Hwei Tai, Chin-Hsien Lin, and Wen-Shian Lu. 2011. Minimal detectable change of the timed “up & go” test and the dynamic gait index in people with Parkinson disease. *Physical therapy* 91, 1 (2011), 114–121.
- [23] TEXAS INSTRUMENTS. 2020. <https://www.tij.co.jp/jp/lit/wp/spyy005a/spyy005a.pdf>
- [24] Joseph Jankovic and Mark Stacy. 2007. Medical management of levodopa-associated motor complications in patients with Parkinson's disease. *CNS drugs* 21 (2007), 677–692.
- [25] Xinrui Jiang, Ye Zhang, Qi Yang, Bin Deng, and Hongqiang Wang. 2020. Millimeter-wave array radar-based human gait recognition using multi-channel three-dimensional convolutional neural network. *Sensors* 20, 19 (2020), 5466.
- [26] Anna Krajushkina, Sven Nomm, Aaro Toomela, Kadri Medijainen, Eveli Tamm, Martti Vaske, Dan Uvarov, Hedi Kahar, Marita Nugis, and Pille Taba. 2018. Gait Analysis Based Approach for Parkinson's Disease Modeling with Decision Tree Classifiers. In *2018 IEEE International Conference on Systems, Man, and Cybernetics (SMC)*. IEEE, 3720–3725.
- [27] Hyeokhyen Kwon, Gari D Clifford, Imari Genias, Doug Bernhard, Christine D Esper, Stewart A Factor, and J Lucas McKay. 2023. An explainable spatial-temporal graphical convolutional network to score freezing of gait in parkinsonian patients. *Sensors* 23, 4 (2023), 1766.
- [28] Zeshui Li, Yang Pan, Haipeng Dai, Wenhao Zhang, Zhen Li, Wei Wang, and Guihai Chen. [n. d.]. PD-Gait: Contactless and privacy-preserving gait measurement of Parkinson's disease patients using acoustic signals. *Software: Practice and Experience* ([n. d.]).
- [29] Beata Lindholm, Maria H Nilsson, Oskar Hansson, and Peter Hagell. 2018. The clinical significance of 10-m walk test standardizations in Parkinson's disease. *Journal of neurology* 265 (2018), 1829–1835.
- [30] Yingcheng Liu, Guo Zhang, Christopher G Tarolli, Rumen Hristov, Stella Jensen-Roberts, Emma M Waddell, Taylor L Myers, Meghan E Pawlik, Julia M Soto, Renee M Wilson, et al. 2022. Monitoring gait at home with radio waves in Parkinson's disease: A marker of severity, progression, and medication response. *Science Translational Medicine* 14, 663 (2022), eadc9669.
- [31] National Institute of Neurological Disorders and Stroke. 2019. <https://www.ninds.nih.gov/health-information/disorders/parkinsons-disease>
- [32] Mandy Lu, Kathleen Poston, Adolf Pfefferbaum, Edith V Sullivan, Li Fei-Fei, Kilian M Pohl, Juan Carlos Niebles, and Ehsan Adeli. 2020. Vision-based estimation of MDS-UPDRS gait scores for assessing Parkinson's disease motor severity. In *Medical Image Computing and Computer Assisted Intervention—MICCAI 2020: 23rd International Conference, Lima, Peru, October 4–8, 2020, Proceedings, Part III* 23. Springer, 637–647.
- [33] Scott M Lundberg, Bala Nair, Monica S Vavilala, Mayumi Horibe, Michael J Eisses, Trevor Adams, David E Liston, Daniel King-Wai Low, Shu-Fang Newman, Jerry Kim, et al. 2018. Explainable machine-learning predictions for the prevention of hypoxaemia during surgery. *Nature biomedical engineering* 2, 10 (2018), 749–760.
- [34] MR Luquin, O Scipioni, J Vaamonde, O Gershoni, and José A Obeso. 1992. Levodopa-induced dyskinesias in Parkinson's disease: clinical and pharmacological classification. *Movement disorders: official journal of the Movement Disorder Society* 7, 2 (1992), 117–124.
- [35] Deval Mehta, Umar Asif, Tian Hao, Erhan Bilal, Stefan Von Cavallar, Stefan Harrer, and Jeffrey Rogers. 2021. Towards automated and marker-less Parkinson disease assessment: predicting UPDRS scores using sit-stand videos. In *Proceedings of the IEEE/CVF Conference on Computer Vision and Pattern Recognition*. 3841–3849.
- [36] Zhen Meng, Song Fu, Jie Yan, Hongyuan Liang, Anfu Zhou, Shilin Zhu, Huadong Ma, Jianhua Liu, and Ning Yang. 2020. Gait recognition for co-existing multiple people using millimeter wave sensing. In *Proceedings of the AAAI Conference on Artificial Intelligence*, Vol. 34.

- 849–856.
- [37] An Nguyen, Nils Roth, Nooshin Haji Ghassemi, Julius Hannink, Thomas Seel, Jochen Klucken, Heiko Gassner, and Bjoern M Eskofier. 2019. Development and clinical validation of inertial sensor-based gait-clustering methods in Parkinson’s disease. *Journal of neuroengineering and rehabilitation* 16 (2019), 1–14.
  - [38] Mario Nieto-Hidalgo and Juan Manuel García-Chamizo. 2017. Classification of pathologies using a vision based feature extraction. In *Ubiquitous Computing and Ambient Intelligence: 11th International Conference, UCAmI 2017, Philadelphia, PA, USA, November 7–10, 2017, Proceedings*. Springer, 265–274.
  - [39] Muhammed Zahid Ozturk, Chenshu Wu, Beibei Wang, and KJ Ray Liu. 2021. GaitCube: Deep data cube learning for human recognition with millimeter-wave radio. *IEEE Internet of Things Journal* 9, 1 (2021), 546–557.
  - [40] R Pahwa, SA Factor, KE Lyons, WG Ondo, G Gronseth, H Bronte-Stewart, M Hallett, J Miyasaki, J Stevens, and WJ Weiner. 2006. Practice Parameter: Treatment of Parkinson disease with motor fluctuations and dyskinesia (an evidence-based review):[RETIRED]: Report of the Quality Standards Subcommittee of the American Academy of Neurology. *Neurology* 66, 7 (2006), 983–995.
  - [41] Sameera Palipana, Dariush Salami, Luis A Leiva, and Stephan Sigg. 2021. Pantomime: Mid-air gesture recognition with sparse millimeter-wave radar point clouds. *Proceedings of the ACM on Interactive, Mobile, Wearable and Ubiquitous Technologies* 5, 1 (2021), 1–27.
  - [42] International Parkinson and Movement Disorder Society. 2008. [https://www.movementdisorders.org/MDS-Files1/PDFs/Rating-Scales/MDS-UPDRS\\_English\\_FINAL.pdf](https://www.movementdisorders.org/MDS-Files1/PDFs/Rating-Scales/MDS-UPDRS_English_FINAL.pdf)
  - [43] RM Pinder, RN Brogden, Phyllis R Sawyer, TM Speight, and GS Avery. 1976. Levodopa and decarboxylase inhibitors: a review of their clinical pharmacology and use in the treatment of parkinsonism. *Drugs* 11 (1976), 329–377.
  - [44] Wasifur Rahman, Masum Hasan, Md Saiful Islam, Titilayo Olubajo, Jeet Thaker, Abdel-Rahman Abdelkader, Phillip Yang, Henry Paulson, Gulin Oz, Alexandra Durr, et al. 2023. Auto-Gait: Automatic Ataxia Risk Assessment with Computer Vision from Gait Task Videos. *Proceedings of the ACM on Interactive, Mobile, Wearable and Ubiquitous Technologies* 7, 1 (2023), 1–19.
  - [45] Claudia Ramaker, Johan Marinus, Anne Margarethe Stigglbout, and Bob Johannes Van Hilten. 2002. Systematic evaluation of rating scales for impairment and disability in Parkinson’s disease. *Movement disorders: official journal of the Movement Disorder Society* 17, 5 (2002), 867–876.
  - [46] Margaret Schenkman, Miriam Morey, and Maggie Kuchibhatla. 2000. Spinal flexibility and balance control among community-dwelling adults with and without Parkinson’s disease. *The Journals of Gerontology Series A: Biological Sciences and Medical Sciences* 55, 8 (2000), M441–M445.
  - [47] Ann-Kathrin Seifert, Moeness G Amin, and Abdelhak M Zoubir. 2019. Toward unobtrusive in-home gait analysis based on radar micro-Doppler signatures. *IEEE Transactions on Biomedical Engineering* 66, 9 (2019), 2629–2640.
  - [48] Ann-Kathrin Seifert, Dominik Reinhard, Abdelhak M Zoubir, and Moeness G Amin. 2019. A robust and sequential approach for detecting gait asymmetry based on radar micro-Doppler signatures. In *2019 27th European Signal Processing Conference (EUSIPCO)*. IEEE, 1–5.
  - [49] Djordje Slijepcevic, Fabian Horst, Sebastian Lapuschkin, Brian Horsak, Anna-Maria Raberger, Andreas Kranz, Wojciech Samek, Christian Breiteneder, Wolfgang Immanuel Schöllhorn, and Matthias Zeppelzauer. 2021. Explaining machine learning models for clinical gait analysis. *ACM Transactions on Computing for Healthcare (HEALTH)* 3, 2 (2021), 1–27.
  - [50] Olumide Sofuwa, Alice Nieuwboer, Kaat Desloovere, Anne-Marie Willems, Fabienne Chavret, and Ilse Jonkers. 2005. Quantitative gait analysis in Parkinson’s disease: comparison with a healthy control group. *Archives of physical medicine and rehabilitation* 86, 5 (2005), 1007–1013.
  - [51] Mary Thompson and Ann Medley. 1998. Performance of individuals with Parkinson’s disease on the Timed Up & Go. *Journal of neurologic physical therapy* 22, 1 (1998), 16–21.
  - [52] Donna M Urquhart, Meg E Morris, and Robert Iansek. 1999. Gait consistency over a 7-day interval in people with Parkinson’s disease. *Archives of physical medicine and rehabilitation* 80, 6 (1999), 696–701.
  - [53] Philip van Dorp and FCA Groen. 2008. Feature-based human motion parameter estimation with radar. *IET Radar, Sonar & Navigation* 2, 2 (2008), 135–145.
  - [54] Tanmay Tulsidas Verlekar, Paulo Lobato Correia, and Luís Ducla Soares. 2018. Using transfer learning for classification of gait pathologies. In *2018 IEEE international conference on bioinformatics and biomedicine (BIBM)*. IEEE, 2376–2381.
  - [55] Ferdous Wahid, Rezaul K Begg, Chris J Hass, Saman Halgamuge, and David C Ackland. 2015. Classification of Parkinson’s disease gait using spatial-temporal gait features. *IEEE journal of biomedical and health informatics* 19, 6 (2015), 1794–1802.
  - [56] Qinghui Wang, Wei Zeng, and Xiangkun Dai. 2022. Gait classification for early detection and severity rating of Parkinson’s disease based on hybrid signal processing and machine learning methods. *Cognitive Neurodynamics* (2022), 1–24.
  - [57] Wei Wang, Alex X Liu, and Muhammad Shahzad. 2016. Gait recognition using wifi signals. In *Proceedings of the 2016 ACM International Joint Conference on Pervasive and Ubiquitous Computing*. 363–373.
  - [58] Wikipedia. 2009. <https://en.wikipedia.org/wiki/Kinect>
  - [59] Wikipedia. 2024. [https://en.wikipedia.org/wiki/Preferred\\_walking\\_speed](https://en.wikipedia.org/wiki/Preferred_walking_speed)
  - [60] David A Winter. 1995. Human balance and posture control during standing and walking. *Gait & posture* 3, 4 (1995), 193–214.

- [61] Jingmiao Wu, Jie Wang, Qinghua Gao, Miao Pan, and Haixia Zhang. 2021. Path-independent device-free gait recognition using mmwave signals. *IEEE Transactions on Vehicular Technology* 70, 11 (2021), 11582–11592.
- [62] Wei Xu, ZhiWen Yu, Zhu Wang, Bin Guo, and Qi Han. 2019. Acousticid: gait-based human identification using acoustic signal. *Proceedings of the ACM on Interactive, Mobile, Wearable and Ubiquitous Technologies* 3, 3 (2019), 1–25.
- [63] Yang Xu, Wei Yang, Jianxin Wang, Xing Zhou, Hong Li, and Liusheng Huang. 2018. WiStep: Device-free step counting with WiFi signals. *Proceedings of the ACM on Interactive, Mobile, Wearable and Ubiquitous Technologies* 1, 4 (2018), 1–23.
- [64] Zhaojun Xue, Dong Ming, Wei Song, Baikun Wan, and Shijiu Jin. 2010. Infrared gait recognition based on wavelet transform and support vector machine. *Pattern recognition* 43, 8 (2010), 2904–2910.
- [65] Xin Yang, Jian Liu, Yingying Chen, Xiaonan Guo, and Yucheng Xie. 2020. MU-ID: Multi-user identification through gaits using millimeter wave radios. In *IEEE INFOCOM 2020-IEEE Conference on Computer Communications*. IEEE, 2589–2598.
- [66] Hanbin Zhang, Chenhan Xu, Huiming Li, Aditya Singh Rathore, Chen Song, Zhiheng Yan, Dongmei Li, Feng Lin, Kun Wang, and Wenyao Xu. 2019. Pdmove: Towards passive medication adherence monitoring of parkinson's disease using smartphone-based gait assessment. *Proceedings of the ACM on interactive, mobile, wearable and ubiquitous technologies* 3, 3 (2019), 1–23.
- [67] Peijun Zhao, Chris Xiaoxuan Lu, Jianan Wang, Changhao Chen, Wei Wang, Niki Trigoni, and Andrew Markham. 2019. mid: Tracking and identifying people with millimeter wave radar. In *2019 15th International Conference on Distributed Computing in Sensor Systems (DCOSS)*. IEEE, 33–40.
- [68] Efthymios Ziagkas, Andreas Loukovitis, Dimitrios Xypolias Zekakos, Thomas Duc-Phu Chau, Alexandros Petrelis, and George Grouios. 2021. A novel tool for gait analysis: Validation study of the smart insole podosmart®. *Sensors* 21, 17 (2021), 5972.